### 3.4. Correlations between the measurements

Linear regression analyses revealed that TNF- production in OVA-stimulated spleen cells correlated significantly with IFN- [$r$=0.832 ($P$=0.001)], confirming that IFN- production in immune cells is regulated, at least in part, by TNF- (Table 1). Anti-OVA-specific serum $IgG_1$ was significantly correlated with IL-6 [$r$=0.657 ($P$=0.010)], TNF- [$r$=0.593 ($P$=0.025)] and INF- [$r$=0.565 ($P$=0.035)]. Significant correlations were also observed between total $IgG_1$ and anti-OVA-specific $IgG_1$ [$r$=0.591 ($P$=0.026)], and between total IgM and anti-OVA-specific IgM [$r$=0.745 ($P$=0.002)].

## 4. Discussion

The results of the present study demonstrate that 7 nAChRs expressed in immune cells are involved in negative regulation of $IgG_1$ antibody production. The significant correlations of serum anti-OVA-specific $IgG_1$ with TNF- , INF- and IL-6 secreted from activated spleen cells suggest that 7 nAChRs exert their effects on $IgG_1$ production via modification of cytokine synthesis in immune cells, at least in part. While both total serum IgM and anti-OVA-specific IgM were found to be increased in 7 KO mice, their levels did not correlate with any cytokines in the present study, suggesting that the serum levels of total serum IgM and anti-OVA-specific IgM at 2 wk after the primary immunization are no more regulated by these cytokines produced in spleen cells.

The level of total serum $IgG_1$ in both 7 KO and wild-type mice was more than 100 times that of anti-OVA-specific $IgG_1$ at 2 wk after the primary immunization, suggesting that the level of total serum $IgG_1$ reflects the pre-immune state. Since the level of total serum $IgG_1$ was significantly higher in 7 KO than wild-type mice, it appears that the level of total serum $IgG_1$ is already higher in 7 KO than wild-type mice even at the pre-immune state. Contrary to our findings, Skok et al. (2005) found a lower level of IgG in pre-immunization serum of 4, 7 or 2 KO mice compared with wild-type mice. Furthermore, they (2006) reported the role of 7 nAChRs in the development of B cells in the bone marrow and proliferation of T and B cells in the spleen, suggesting the involvement of 7 nAChRs in positive regulation of B cell function. The reasons for the discrepancies on the role of 7 nAChRs in the regulation of immune cell function between the studies by Skok et al. (2005, 2006) and the present study remain to be clarified.

Using 7 KO mice, Wang et al. (2003) showed that nicotine prevents lipopolysaccharide-induced septic shock by inhibiting synthesis and release of tumor necrosis factor (TNF)- , a pro-inflammatory cytokine, in macrophages through 7 nAChR-mediated pathways and confirmed essential role of 7 nAChRs in the regulation of inflammatory responses. The spleen cells used in the present study consisted of T and B cells and monocytes containing macrophages and DCs. The higher TNF- release from the antigen-stimulated spleen cells in 7 KO than wild-type mice is in line with the results observed by Wang et al. (2003). Perhaps, ACh produced either by the antigen-activated T cells or DCs suppresses TNF- release through stimulation of 7 nAChRs in spleen cells of wild-type mice. However, the level of ChAT mRNA expression in the spleen cells was below the detection limit of RT-PCR with ethidium bromide staining. Vasoactive intestinal polypeptide (VIP) selectively increases the affinity of the agonist for nAChRs through action on VIP receptors, VPAC1 and VPAC2 (Liu et al., 2000). Spleen cells used in the present study express mRNAs for VIP as well as VPAC1 and VPAC2 (Kawashima et al., 2007). These findings suggest that even a small amount of ACh should be able to activate 7 nAChRs and suppress TNF- release in the presence of VIP.

Secreted mammalian Ly-6/urokinase plasminogen-type activator receptor-related protein (SLURP)-1, a member of the Ly-6/uPAR protein superfamily, has been isolated from human blood and urine (Adermann et al., 1999) and found to potentiate the amplitude of the ACh-induced macroscopic currents in *Xenopus* oocytes expressing the human 7 nAChRs acting as an allosteric agonist (Chimienti et al., 2003). Arredondo et al. (2005) have shown that SLURP-1 competes with nicotine for binding to 7 nAChRs on human keratinocytes and directly induces various biochemical and functional effects such as increases of caspase-3 and-8 activities and enhancement of pro-apototic activity, suggesting that SLURP-1 has the possibility to serve as an endogenous agonist for human keratinocyte 7 nAChRs. Furthermore, Moriwaki et al. (2007) demonstrated the expression of mRNA for SLURP-1 in various tissues and organs including the spleen and thymus as well as T and B cells, DCs and macrophages of C57BL/6J mice. Collectively, these findings suggest that even a small amount of ACh can effectively activate 7 nAChRs in the presence of SLURP-1 acting as an allosteric agonist, or that SLURP-1 itself acting as an agonist stimulates 7 nAChRs, leading to suppression of synthesis and release of TNF- in spleen cells under the present experimental conditions.

Antigen-activated spleen cell cultures of 7 KO mice contained higher levels of TNF- , IFN- and IL-6 than those of the wild-type mice (Fig. 3). Macrophages, DCs and monocytes can collectively synthesize and release these cytokines in response to specific antigenic stimulation and subsequently become activated in response to them. The major source of the TNF- in the present study appears to be splenic $CD14^+$ cells (monocytes, macrophages and DCs) comprised of 10% of spleen cells. Furthermore, activated $CD4^+$ T and B cells, comprised of 30% and 45% of spleen cells, respectively, can also synthesize TNF- . TNF- with IL-2 stimulates synthesis and release of INF- from activated T cells and DCs, which, in turn, activates phagocytosis by macrophages, and facilitates antigen recognition by T and B cells, leading to facilitation of antibody synthesis (Becher et al., 1999). Exposure of activated $CD4^+$ and $CD8^+$ T cells, macrophages and DCs to TNF- promotes synthesis of IL-6 that induces the final maturation of B cells into antibody-producing cells (Akira et al., 1993; Hirano, 1998; Kopf et al., 1998). These findings suggest that proinflammatory cytokines, such as TNF- , IFN- and IL-6 individually have stimulatory effects on the humoral responses to various antigenic stimuli (Khan et al., 2002). Significant correlations of anti-OVA-specific $IgG_1$ with TNF- , IFN- and IL-6 (Table 1)

support the above findings. Therefore, elevated total serum $IgG_1$ and anti-OVA-specific $IgG_1$, and somewhat increases in total serum IgM and anti-OVA-specific IgM in 7 KO mice observed in the present study could be ascribed to the disinhibition of TNF- release from immune cells due to 7 nAChR deficiency leading to facilitation of IFN- and IL-6 production.

In our previous study with $M_1/M_5$ KO mice (Fujii et al., in press), we found a slight but significant suppression of AChE gene expression, suggesting that either $M_1$ and/or $M_5$ mAChR signaling modulates AChE transcription, though the precise mechanism remained unclear. Since we did not find any difference in the level of AChE gene expression between the genotypes in the present study, AChE expression appears to be independent of 7 nAChRs.

In conclusion, 7 nAChRs are involved in negative regulation of immune cell function by inhibiting synthesis and release of proinflammatory cytokines, such as TNF- , IFN- and IL-6 in spleen cells, leading to suppression of $IgG_1$ production. The results of the present study along with our previous findings on the role of $M_1$ and/or $M_5$ mAChRs involved in positive regulation of IL-6 production (Fujii et al., in press) support the notion that non-neuronal cholinergic system expressed in immune cells is involved in the regulation of immune function via both nAChRs- and mAChRs-mediated pathways.

## References


Adermann, K., Wattler, F., Wattler, S., Heine, G., Meyer, M., Forssmann, W.-G., Nehls, M., 1999. Structural and phylogenetic characterization of human SLURP-1, the first secreted mammalian member of the Ly-6/uPAR protein superfamily. Protein Sci. 8, 810–819.

Akira, S., Taga, T., Kishimoto, T., 1993. Interleukin-6 in biology and medicine. Adv. Immunol. 54, 1–78.

Arredondo, J., Chernyavsky, A.I., Webber, R.J., Grando, S.A., 2005. Biological effects of SLURP-1 on human keratinocytes. J. Invest. Dermatol. 125, 1236–1241.

Becher, B., Blain, M., Giacomini, P.S., Antel, J.P., 1999. Inhibition Th1 polarization by soluble TNF receptor is dependent on antigen-presenting cell-derived IL-12. J. Immunol. 162, 684–688.

Chimienti, F., Hogg, R.C., Plantard, L., Lehmann, C., Brakch, N., Fischer, J., Huber, M., Bertrand, D., Hohl, D., 2003. Identification of SLURP-1 as an epidermal neuromodulator explains the clinical phenotype of Mal de Meleda. Hum. Mol. Genet. 12, 3017–3024.

Fujii, T., Kawashima, K., 2001. The non-neuronal cholinergic system: an independent non-neuronal cholinergic system in lymphocytes. Jpn. J. Pharmacol. 85, 11–15.

Fujii, T., Yamada, S., Watanabe, Y., Misawa, H., Tajima, S., Fujimoto, K., Kasahara, T., Kawashima, K., 1998. Induction of choline acetyltransferase mRNA in human mononuclear leukocytes stimulated by phytohemagglutinin, a T-cell activator. J. Neuroimmunol. 82, 101–107.

Fujii, Y.X., Tashiro, A., Arimoto, K., Fujigaya H., Yoshikawa, K., Moriwaki, Y., Misawa, H., Fujii, T., Matsui, M., Kasahara, T., Kawashima, K., in press. Diminished antigen-specific $IgG_1$ and interleukin-6 production and acetylcholinesterase expression in combined $M_1$ and $M_5$ muscarinic acetylcholine receptor knockout mice. J. Neuroimmunol.

Hirano, T., 1998. Interleukin 6 and its receptor: ten year later. Int. Rev. Immunol. 16, 249–284.

Kawashima, K., Fujii, T., 2000. Extraneuronal cholinergic system in lymphocytes. Pharmacol. Ther. 86, 29–48.

Kawashima, K., Fujii, T., 2003a. The lymphocytic cholinergic system and its biological function. Life Sci. 72, 2101–2109.

Kawashima, K., Fujii, T., 2003b. The lymphocytic cholinergic system and its contribution to the regulation of immune activity. Life Sci. 74, 675–696.

Kawashima, K., Fujii, T., 2004. Expression of non-neuronal acetylcholine in lymphocytes and its contribution to the regulation of immune function. Front. Biosci. 9, 2063–2085.

Kawashima, K., Yoshikawa, K., Fujii, Y.X., Moriwaki, Y., Misawa, H., 2007. Expression and function of genes encoding cholinergic components in murine immune cells. Life Sci. 80, 2314–2319.

Khan, A.Q., Shen, Y., Wu, Z.-Q., Wynn, T.A., Snapper, C.M., 2002. Endogenous pro- and anti-inflammatory cytokines differentially regulates an in vivo humoral response to *Streptococcus pneumoniae*. Infect. Immun. 70, 749–761.

Kimura, R., Ushiyama, N., Fujii, T., Kawashima, K., 2003. Nicotine-induced $Ca^{2+}$ signaling and down-regulation of nicotinic acetylcholine receptor subunit expression in the CEM human leukemic T-cell line. Life Sci. 72, 2155–2159.

Kopf, M., Herren, S., Wiles, M.V., Pepys, M.B., Kosco-Vilbois, M.H., 1998. Interleukin 6 influences germinal center development and antibody production via a contribution of C3 complement component. J. Exp. Med. 188, 1895–1906.

Kuo, Y., Lucero, L., Michaels, J., DeLuca, D., Lukas, R.J., 2002. Differential expression of nicotinic acetylcholine receptor subunits in fetal and neonatal mouse thymus. J. Neuroimmunol. 130, 140–154.

Liu, D.M., Cuevas, J., Adams, D.J., 2000. VIP and PACAP potentiation of nicotinic ACh-evoked currents in rat parasympathetic neurons is mediated by G-protein activation. Eur. J. Neurosci. 12, 2243–2251.

Moriwaki, Y., Yoshikawa, K., Fukuda, H., Fujii, Y.X., Misawa, H., Kawashima, K., 2007. Immune system expression of SLURP-1 and SLURP-2, two endogenous nicotinic acetylcholine receptor ligands. Life Sci. 80, 2365–2368.

Orr-Urtreger, A., Goldner, F.M., Saeki, M., Lorenzo, I., Goldberg, L., De Biasi, M., Dani, J.A., Patrick, J.W., Beaudet, A.L., 1997. Mice deficient in the 7 neuronal nicotinic acetylcholine receptor lack -bungarotoxin binding sites and hippocampal fast nicotinic currents. J. Neurosci. 17, 9165–9178.

Skok, M.V., Grailhe, R., Changeux, J.-P., 2005. Nicotinic receptors regulate B lymphocyte activation and immune response. Eur. J. Pharmacol. 517, 246–251.

Skok, M.V., Grailhe, R., Agenes, F., Changeux, J.-P., 2006. The role of nicotinic acetylcholine receptors in lymphocyte development. J. Neuroimmunol. 171, 86–98.

Sopori, M., 2002. Effects of cigarette smoke on immune system. Nat. Rev. Immunol. 2, 372–377.

Wang, H., Yu, M., Ochani, M., Amella, C.A., Tanovic, M., Susaria, S., Li, J.H., Wang, H., Yang, H., Ulloa, L., Al-Abed, Y., Czura, C.J., Tracey, K.J., 2003. Nicotinic acetylcholine receptor 7 subunit is an essential regulator of inflammation. Nature 421, 384–388.

# Renal defects associated with improper polarization of the CRB and DLG polarity complexes in MALS-3 knockout mice

Olav Olsen,[1] Lars Funke,[1] Jia-fu Long,[4] Masaki Fukata,[1] Toshinari Kazuta,[1] Jonathan C. Trinidad,[3] Kimberly A. Moore,[2] Hidemi Misawa,[1] Paul A. Welling,[5] Alma L. Burlingame,[3] Mingjie Zhang,[4] and David S. Bredt[1,6]

[1]Departments of Physiology, [2]Cellular and Molecular Pharmacology, and [3]Pharmaceutical Chemistry, University of California, San Francisco, San Francisco, CA 94143
[4]Department of Biochemistry, Molecular Neuroscience Center, Hong Kong University of Science and Technology, Clear Water Bay, Kowloon, Hong Kong
[5]Department of Physiology, University of Maryland School of Medicine, Baltimore, MD 21201
[6]Department of Integrative Biology, Eli Lilly and Company, Indianapolis, IN 46285

Kidney development and physiology require polarization of epithelia that line renal tubules. Genetic studies show that polarization of invertebrate epithelia requires the crumbs, partition-defective-3, and discs large complexes. These evolutionarily conserved protein complexes occur in mammalian kidney; however, their role in renal development remains poorly defined. Here, we find that mice lacking the small PDZ protein mammalian LIN-7c (MALS-3) have hypomorphic, cystic, and fibrotic kidneys. Proteomic analysis defines MALS-3 as the only known core component of both the crumbs and discs large cell polarity complexes. MALS-3 mediates stable assembly of the crumbs tight junction complex and the discs large basolateral complex, and these complexes are disrupted in renal epithelia from *MALS-3* knockout mice. Interestingly, MALS-3 controls apico-basal polarity preferentially in epithelia derived from metanephric mesenchyme, and defects in kidney architecture owe solely to MALS expression in these epithelia. These studies demonstrate that defects in epithelial cell polarization can cause cystic and fibrotic renal disease.

## Introduction

Polarity is a physical attribute of most eukaryotic cells that is indispensable for their function. Generation and maintenance of cell polarity requires the active segregation of molecular components and imparts distinct properties to subcellular domains. Polarization occurs along a major axis in epithelia, neurons, and asymmetrically dividing cells. In epithelia, polarization relative to the tight junction functionally separates the apical and basolateral domains; neuronal polarization allows for differential development of dendrites and axons. During asymmetric cell division, a polarity cue in the mother cell directs distribution of cell fate determinants in daughter cells. In all these cases, failure to establish cell polarity compromises tissue differentiation and function.

Sustained polarization of epithelial cells lining renal tubules is essential for kidney development and function (Campo et al., 2005). Tubules in the permanent kidney develop through reciprocal interactions between the ureteric bud and metanephric mesenchyme (Dressler, 2006). The ureteric bud invades the metanephros and undergoes a series of branching events that give rise to the collecting duct system. In response to signals released from ureteric bud tips, mesenchymal cells transform into polarized epithelia, which differentiate into the tubule cells along the remainder of the nephron. Epithelial cell polarization relies on tight junctions, which connect tubule cells, provide paracellular barriers to ion and fluid movement, and organize the membrane into apical and basolateral domains (Schneeberger and Lynch, 1992; Van Itallie and Anderson, 2004; Shin et al., 2006). Polarized expression of channels and transporters allows for vectorial transport of solutes along the nephron, resulting in physiological urine formation. Aberrations in epithelial cell polarity are implicated in the pathogenesis of renal cysts, renal fibrosis, and renal failure (Kalluri and Neilson, 2003; D.B. Lee et al., 2006); however, the molecular mechanisms underlying these complex diseases remain poorly understood.

O. Olsen and L. Funke contributed equally to this paper.

Correspondence to Olav Olsen: olav.olsen@ucsf.edu; or David S. Bredt: bredt@lilly.com

Abbreviations used in this paper: CRB, Crumbs; DLG, Discs large; LGL, lethal giant larvae; MAGUK, membrane-associated guanylate kinase; MALS-3, mammalian LIN-7c; MMKO, metanephric mesenchyme KO; PALS, proteins associated with LIN-7; PAR-3, partition-defective-3; PATJ, PALS-associated tight junction; SCRIB, scribble; UBKO, ureteric bud KO.

The online version of this article contains supplemental material.

The Rockefeller University Press $30.00
http://www.jcb.org/cgi/doi/10.1083/jcb.200702054

Supplemental Material can be found at:
http://www.jcb.org/cgi/content/full/jcb.200702054/DC1

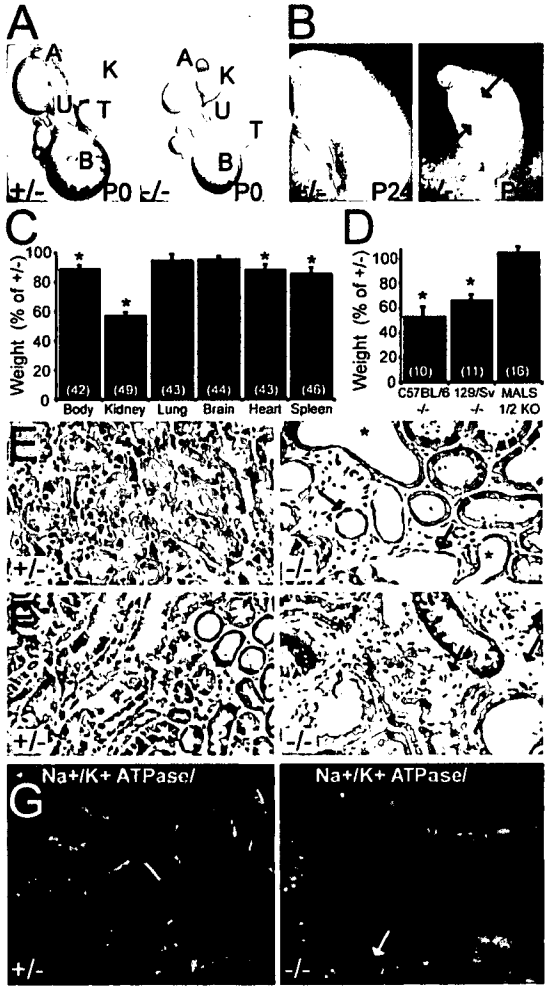


Figure 1. ***MALS-3*** **mice display renal defects.** (A) Dissected urinary tracts from P0 pups show significantly smaller kidneys in *MALS-3* knockout (/) mice as compared with heterozygote (/) littermates. A, adrenal gland; B, bladder; K, kidney; T, testis; U, ureter. (B) Kidneys from adult *MALS-3* mice are hypoplasic, dysplasic, and cystic; arrows mark cysts. (C) Quantification of body and organ weight of adult *MALS-3* mice and littermates. Kidneys from *MALS-3* are significantly smaller (57.9% 1.8; $P < 0.01$). (D) *MALS-3* mice backcrossed to 129/Sv or C57BL/6 for 8 generations show reduced kidney size (64.8% 3.2; $P < 0.01$ or 53.4% 8.5; $P < 0.01$, respectively). Mice lacking both MALS-1 and MALS-2 (MALS 1/2 KO) have normal kidneys. For C and D the number of animals is within the parentheses. (E) Hematoxylin and eosin stained kidney section from a 6-wk-old *MALS-3* mouse shows normal arrangement of densely packed tubules (left). Kidney from a *MALS-3* littermate shows marked tubulointerstitive changes, including dilatation of tubular lumina, tubular dedifferentiation, and fibrosis (right). Asterisks mark tubules with epithelia undergoing dedifferentiation, and arrows show dedifferentiated tubules. (F) Trichrome stained kidney section from a 6-wk-old *MALS-3* mouse displays little or no collagen deposition (left). In contrast, a kidney from a *MALS-3* littermate stains bright blue (arrows), revealing extensive fibrosis (right). (G) Immunolocalization of the $Na^+/K^+$ ATPase shows basolateral membrane localization in renal tubules of *MALS-3* mice (left). Polarized expression of the $Na^+/K^+$ ATPase is lost (arrows) in renal tubules undergoing simplification in *MALS-3* mice.

Genetic studies of invertebrates have identified two conserved tight junction PDZ protein complexes, the Crumbs (CRB) and partition-defective-3 (PAR-3) complexes, which contribute to cell polarity (Tepass et al., 1990; Etemad-Moghadam et al., 1995; Watts et al., 1996; Tabuse et al., 1998; Bachmann et al., 2001; Hong et al., 2001; Djiane et al., 2005). CRB is a transmembrane protein (Tepass et al., 1990), whose C-terminus binds to the PDZ domain of PALS (Roh et al., 2002) or PATJ (Bhat et al., 1999). In turn, PALS and PATJ bind one another through heterodimerization of their L27 domains (Roh et al., 2002). The CRB complex is an apical membrane determinant that stabilizes the apical membrane cytoskeleton through interaction with -spectrin and D-moesin (Medina et al., 2002). The second complex includes the PDZ protein PAR-3, which binds to atypical protein kinase C (aPKC) (Izumi et al., 1998), and the PDZ protein PAR-6 (Joberty et al., 2000; Lin et al., 2000). This PAR-3 complex excludes certain basolateral proteins from the apical domain via aPKC phosphorylation (Betschinger et al., 2003; Plant et al., 2003). The CRB and PAR-3 polarity complexes were originally thought to act independently, but physical and functional interactions between these complexes establish cell polarity (Hurd et al., 2003).

Genetic analyses of invertebrates also identified several basolateral proteins required for epithelial cell polarization. Discs large (*dlg*) (Woods and Bryant, 1991), lethal giant larvae (*lgl*) (Gateff and Schneiderman, 1969), and scribble (*scrib*) (Bilder and Perrimon, 2000; Bilder et al., 2000) were originally identified as tumor suppressor genes in *Drosophila*. Mutations in *dlg*, *lgl*, or *scrib* disrupt epithelial cell polarity and cause neoplastic overgrowth of tissues. DLG genetically interacts with the multi-PDZ protein SCRIB and the WD40 motif protein LGL (Bilder et al., 2000). Interplay between these basolateral polarity proteins and the apical polarity complexes establish and maintain cellular polarity. For example, LGL is phosphorylated by aPKC, thereby excluding LGL from the apical compartment (Betschinger et al., 2003; Plant et al., 2003).

The mammalian homologue of LIN-7 (MALS) can bind components from both the apical (Kamberov et al., 2000) and basolateral (Kaech et al., 1998; Lee et al., 2002) polarity complexes, suggesting an additional mode for interplay. Three MALS genes occur in mammals, and each is a small protein comprising an L27 and a PDZ domain (Butz et al., 1998; Borg et al., 1999; Jo et al., 1999). The L27 domain links MALS to either the CRB (Kamberov et al., 2000) or DLG (Lee et al., 2002) complex, but a role for MALS in these polarity complexes is unknown. Biochemical and cell biological experiments suggest a variety of possible roles for MALS in mammalian epithelial cell lines. MALS localizes to the basolateral membrane of Madin-Darby canine kidney (MDCK) cells (Perego et al., 1999; Olsen et al., 2002). By analogy to the role of LIN-7 in *Caenorhabditis elegans*, the PDZ domain of MALS may anchor receptors to the basolateral domain of MDCK cells (Straight et al., 2001; Shelly et al., 2003). Alternatively, MALS may stabilize PALS and mediate tight junction formation (Straight et al., 2006). Other studies suggest that MALS interacts with -catenin and mediates organization of adherens junctions (Perego et al., 2000). Finally, MALS can regulate endocytosis or endosomal sorting in epithelial cell lines (Perego et al., 1999; Straight et al., 2001). Despite these numerous suggestions, genetic analyses have yet to identify functions for MALS in mammalian epithelia.

We characterize *MALS-3* knockout (/) mice and identify an essential role for MALS-3 in defining polarity of renal

Table I. **Renal function tests**

| Renal function | ⊠ /⊠ | ⊠ /⊠ |
|---|---|---|
| Uv (ml/day) | 2.26 ⊠ 1.3 | 5.13 ⊠ 2.2* |
| Ccre (ul/min) | 73 ⊠ 16 | 60 ⊠ 11* |
| UNaV (uEq/day) | 106 ⊠ 26 | 180 ⊠ 23* |
| UKV(uEq/day) | 374 ⊠ 103 | 427 ⊠ 59 |
| Uvca (mg/day) | 0.11 ⊠ 0.04 | 0.15 ⊠ 0.04 |
| UPiV (mg/day) | 1.22 ⊠ 0.49 | 0.63 ⊠ 0.08 |
| FENa% | 0.74 ⊠ 0.15 | 1.2 ⊠ 0.09* |
| FEK% | 60 ⊠ 14 | 78 ⊠ 6 |

Creatine clearance (Ccr) was calculated from the plasma (Pcr), urine creatine (Ucr) concentrations, and the urine flow rate (V), Cr ⊠ U ⊠ V/P; Fractional excretion is the amount excreted divided by the amount filtered. *n* ⊠ 4 each. *, $P < 0.05$, *t* test.

Table II. **Plasma chemistry**

| Plasma | ⊠ /⊠ | ⊠ /⊠ |
|---|---|---|
| Na (mEq/l) | 151 ⊠ 2.5 | 151 ⊠ 3.4 |
| K (mEq/l) | 6.6 ⊠ 0.58 | 6.33 ⊠ 0.32 |
| Cl (mEq/l) | 113 ⊠ 3.7 | 110 ⊠ 3.09 |
| Creatinine (mg/dl) | 0.32 ⊠ 0.04 | 0.3 ⊠ 0.0 |
| Ca (mg/dl) | 8.86 ⊠ 0.3 | 9.6 ⊠ 0.12 |
| Pi (mg/dl) | 8.86 ⊠ 0.3 | 7.9 ⊠ 0.35 |
| BUN (mg/dl) | 27 ⊠ 6.69 | 40 ⊠ 5.24* |

*, $P < 0.05$, *t* test.

epithelial cells. *MALS-3*$^{⊠/⊠}$ mice have hypomorphic kidneys characterized by numerous cysts and Abrosis. These developmental defects owe to a loss of polarity speciAcally in epithelia derived from the metanephric mesenchyme. Immunoprecipitation proteomics analysis reveals MALS-3 binds to the CRB tight junction and DLG basolateral complexes. Biochemical studies show the L27 domain of MALS-3 assembles and stabilizes these complexes. In proximal tubule cells from MALS-3 mutant mice, the CRB complex is lost from tight junctions and DLG mislocalizes to tight junctions. These studies demonstrate that MALS-3 organizes these two discrete polarity complexes and that disruption of epithelial cell polarity can result in renal agenesis, cysts, and Abrosis.

## Results

### Kidney pathology in *MALS-3*$^{⊠/⊠}$ mice

Kidneys from neonatal and adult *MALS-3*$^{⊠/⊠}$ mice are noticeably smaller than those from heterozygous (⊠ /⊠ ) littermates (Fig. 1, A and B), and ⊠ 15% of *MALS-3*$^{⊠/⊠}$ display unilateral renal agenesis (unpublished data). Furthermore, *MALS-3*$^{⊠/⊠}$ kidneys are studded with numerous cysts (Fig. 1 B; and Fig. S1 A, available at http://www.jcb.org/cgi/content/full/jcb.200702054/DC1). Most cysts (8 of 11) fail to express tubule segment-speciAc markers, only 1 of 11 cysts stained with a lectin that labels proximal tubules (Fig. S1 B). Kidneys from *MALS-3*$^{⊠/⊠}$ are dramatically reduced in weight relative to *MALS-3*$^{⊠/⊠}$ (Fig. 1 C). Whereas the kidney is reduced by nearly 45%, only a ⊠ 10% reduction in the size of heart, spleen, and overall body weight is observed. Renal hypoplasia occurs in *MALS-3*$^{⊠/⊠}$ mice backcrossed to either the 129/Sv or C57BL/6 strain and is speciAc to *MALS-3*$^{⊠/⊠}$, as kidneys from mice lacking both MALS-1 and MALS-2 are normal in size (Fig. 1 D).

Microscopic analysis of adult and newborn *MALS-3*$^{⊠/⊠}$ kidneys reveals dramatic cellular abnormalities in kidney architecture (Fig. 1 E; Fig. S1 C). *MALS-3*$^{⊠/⊠}$ kidneys display marked tubulointerstitial changes including tubular dilatation and dedifferentiation/simpliAcation (Fig. 1 E). Trichrome staining reveals interstitial Abrosis (Fig. 1 F; Fig. S1 D), a condition characterized by the accumulation of extracellular matrix proteins and Abroblasts, which is a hallmark of end-stage renal disease (Kalluri and Neilson, 2003; J.M. Lee et al., 2006). Renal cysts and Abrosis in *MALS-3*$^{⊠/⊠}$ are accompanied by a loss of epithelial cell polarity. The $Na^{⊠}/K^{⊠}$ ATPase, which is normally localized basolaterally, becomes diffusely localized in dedifferentiated tubular epithelia (Fig. 1 G).

*MALS-3*$^{⊠/⊠}$ mice also manifest defects in renal function (Table I). Compared with *MALS-3*$^{⊠/⊠}$, *MALS-3*$^{⊠/⊠}$ mice exhibit a considerable increase in urine output and sodium excretion. Creatine clearance, a measure of glomerular function, was modestly decreased whereas blood urea nitrogen (BUN) was elevated (Table II). This is likely a consequence of extracellular ⊠uid volume contraction resulting from the polyuria. Urine concentrating ability, measured as the response to 12-h water deprivation and vasopressin injection after a high water load, was also impaired; urine osmolarity only increased 3 ⊠ 0.9-fold (1,024 ⊠ 490 mOsm/l change) in *MALS-3*$^{⊠/⊠}$ mice compared with 7.2 ⊠ 0.9-fold (2,764 mOsm/l ⊠ 332 mOsm/l) in *MALS-3*$^{⊠/⊠}$ (Fig. S1 E). Together with the histopathological observations, these results are reminiscent of nephronophthsis, the most common genetic disorder of progressive renal failure in children.

### MALS-3 localizes to epithelial cells along the length of the nephron

To determine the pathogenesis of these kidney defects, the cellular distribution of MALS-3 protein was examined in kidney sections. MALS-3 is present in epithelial cells of renal tubules but is absent from glomeruli (Fig. 2). In the kidney cortex, MALS-3 occurs in collecting duct epithelia that label for aquaporin-2 (Fig. 2 B) and proximal tubule epithelia that stain intensely for phalloidin (Fig. 2 C). In proximal tubule cells, MALS-3 localizes to the basolateral membrane and the tight junction (Fig. 2, C and D; Fig. S2 A, available at http://www.jcb.org/cgi/content/full/jcb.200702054/DC1). In the inner medulla, MALS-3 is present in tubule cells of the loop of Henle and collecting duct (Fig. 2 E). In collecting duct epithelia, MALS-3 is restricted to the basolateral membrane and is not detected at the tight junction (Fig. 2, F and G). As expected, MALS-3 staining is absent in *MALS-3*$^{⊠/⊠}$ mice (Fig. 2, B, C, E, and F; and Fig. S2 A).

### MALS-3 interacts with apical and basolateral polarity complexes

To define the proteins associated with MALS-3, we conducted immunoprecipitation proteomics. Immunoprecipitation of MALS-3 from adult *MALS-3*$^{⊠/⊠}$ kidney homogenates shows a series of speciAc protein bands that are absent from *MALS-3*$^{⊠/⊠}$ immunoprecipitates (Fig. 3 A). As determined by mass spectroscopy, MALS-3 interacts with several proteins found in complexes

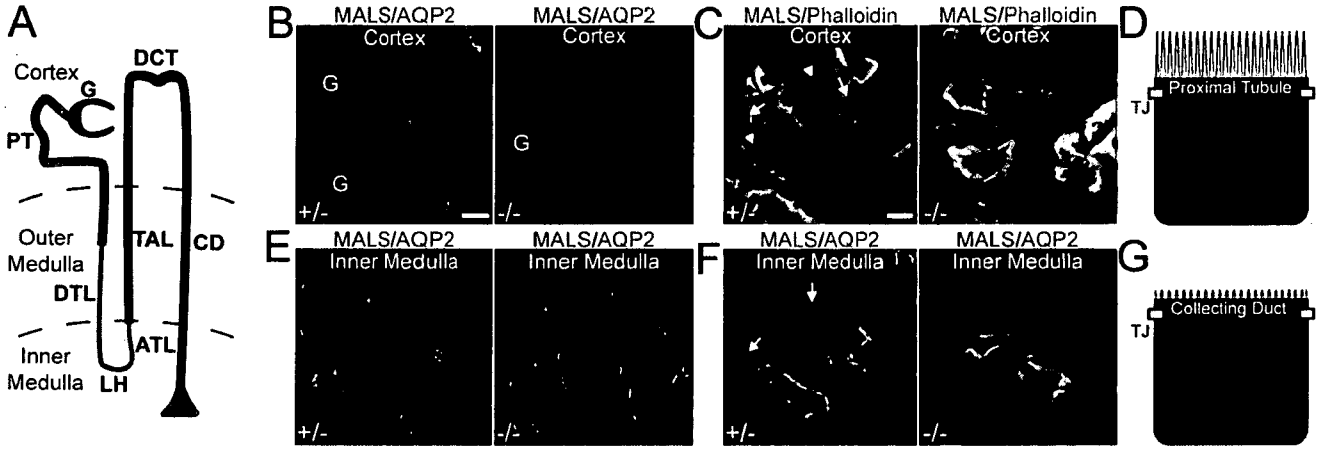


Figure 2. **MALS-3 localizes at the basolateral membrane and tight junction of renal epithelia.** (A) Schematic depicting the arrangement of tubular segments in the kidney. ATL, ascending thin limb; CD, collecting duct; DCT, distal convoluted tubule; DTL, descending thin limb; G, glomerulus; LH, loop of Henle; PT, proximal tubule; TAL, thick ascending limb. (B) Low magnification fluorescent images from the cortex of kidney sections from a 6-wk-old mouse reveal that MALS-3 (red) primarily localizes to the basolateral membrane of tubular structures. MALS-3 staining is absent from *MALS-3*$^{\Delta/\Delta}$. AQP2 (green) specifically labels collecting ducts. (C) High magnification of proximal tubules shows a prominent brush border (phalloidin, green). DAPI (blue) stains nuclei. In proximal tubules, MALS-3 (red) is at both the basolateral membranes (arrowheads) and the tight junctions (arrows). (D) Cartoon summarizing MALS-3 localization in proximal tubules. Brush border and tight junction (TJ) are shown in green and yellow, respectively. (E and F) Low and high magnification images of the inner medulla show basolateral localization (arrows) of MALS-3 in collecting ducts (AQP2 positive tubules; green). (G) Cartoon depicting AQP2 (green) and MALS-3 (red) localizations in collecting ducts. Bars are 50 μm in B and E; 10 μm in C and F.

that determine cell polarity. MALS-3 immunoprecipitates contain DLG and CASK, proteins that localize to the basolateral surface, and PALS-1, PALS-2, PALS-4 (Mpp7), and PATJ, proteins that localize to tight junctions. Western blotting confirmed all of these interactions and demonstrated coimmunoprecipitation of CRB-3, the prototypical tight junction polarity protein, with similar recovery (Fig. 3 B).

To characterize the role of MALS-3 in these polarity complexes, we first assessed protein levels in *MALS-3*$^{\Delta/\Delta}$ kidneys. Strikingly, levels of all components of the CRB-3 tight junction complex are drastically diminished in *MALS-3*$^{\Delta/\Delta}$ kidneys (Fig. 3 C). CRB-3 itself is decreased by 60% and PALS-1 and PATJ are each decreased by ≈ 80% (Fig. 3, C and D). In contrast, aPKCζ and PAR-3, members of a distinct tight junction polarity complex, were unchanged in *MALS-3*$^{\Delta/\Delta}$. Levels of basolateral proteins, LGL, CASK, and DLG are also significantly decreased (Fig. 3, C and D). Structural proteins of the tight junction, claudin-7 and -8, are unaffected in *MALS-3*$^{\Delta/\Delta}$, while ZO-2 is modestly decreased. E-cadherin and β-catenin of the adherens junctions are also unchanged (Fig. 3, C and D). MALS-2 protein is up-regulated in kidneys of *MALS-3*$^{\Delta/\Delta}$, which has also been noted in brains of MALS mutants (Misawa et al., 2001).

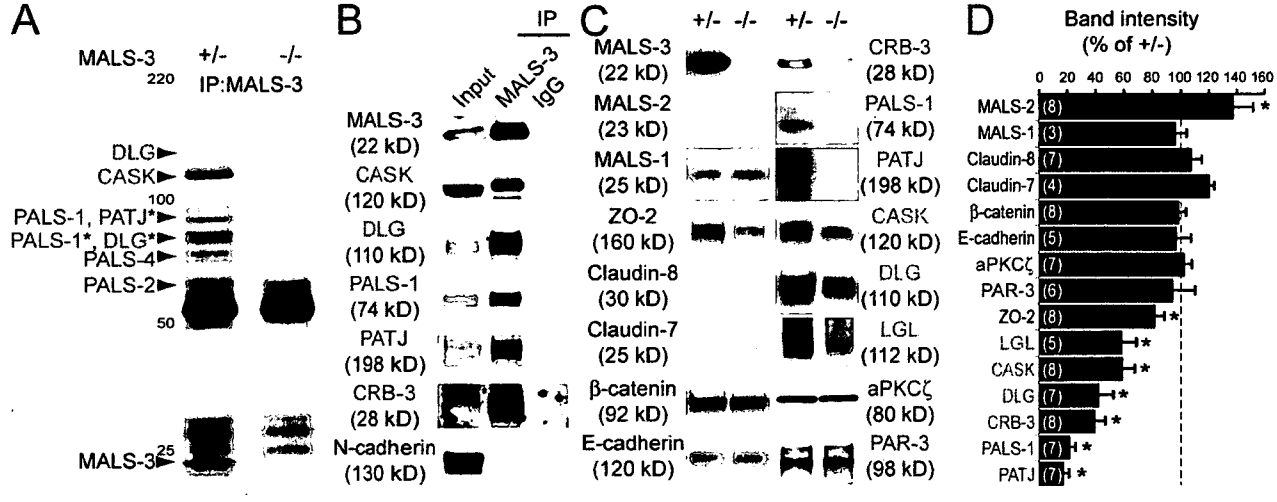


Figure 3. **MALS-3 interacts with both apical and basolateral polarity complexes in the kidney.** (A) Silver staining of kidney extracts immunoprecipitated with anti-MALS-3 antibody shows a series of proteins from *MALS-3*$^{\Delta/\Delta}$ homogenates that are absent from *MALS-3*$^{\Delta/\Delta}$ precipitates. (B) Western blotting of extracts immunoprecipitated with anti-MALS-3 antibody confirms specific association of CASK, DLG, PALS, PATJ, and CRB-3 with MALS-3. (C) Kidney homogenates from *MALS-3*$^{\Delta/\Delta}$ and *MALS-3*$^{\Delta/\Delta}$ mice immunoblotted for numerous proteins associated with MALS-3 and with epithelial cell junctions. (D) Quantification of protein levels in C. The number of blots quantified for each protein is in parentheses. In A–D, proteins of the CRB, PAR-3, and DLG complexes are shown in red, blue, and green, respectively. Asterisks denote P values < 0.05.

### MALS-3 L27 domain mediates assembly of CRB and DLG complexes

Through L27 domain interactions, MALS-3 associates directly with CASK and PALS (Kaech et al., 1998; Kamberov et al., 2000; Lee et al., 2002), which in turn bind to DLG and PATJ (Lee et al., 2002; Roh et al., 2002), respectively. Interestingly, levels of DLG and PATJ, which do not directly bind to MALS-3, are reduced to a greater or similar extent as CASK and PALS (Fig. 3, C and D). This suggests that MALS-3 may mediate cooperative assembly of these L27 domain complexes. To explore this biochemically, the L27 domains of CASK and DLG were expressed in the absence of the MALS L27 domain in bacteria. Under these conditions, the CASK/DLG binary complex is substantially degraded upon isolation and further deteriorated within 24 h at 4□C (Fig. 4 A). Inclusion of the MALS L27 domain promotes formation of a MALS/CASK/DLG L27 complex that is stable for several days at 35□C (Fig. 4 A). Furthermore, the MALS/CASK/DLG ternary complex was more resistant to urea denaturation than either the MALS/CASK or DLG/CASK binary complexes (Fig. 4 B). MALS also stabilized the MALS/PALS/PATJ L27 complex (unpublished data). The oligomeric nature of protein complexes containing four L27 domains has not been determined. NMR showed that the isolated CASK and DLG L27 domains form a "dimer of dimers" structure (Feng et al., 2004), which might imply high order oligomerization of L27 domain complexes containing three proteins. However, gel Altration analysis shows that the MALS/CASK/DLG complex elutes as a single peak corresponding to □ 38 kD (Fig. 4 C), implying a 1:1:1 stoichiometry. Similarly, the tandem PALS L27 domains elute with MALS L27 and PATJ L27 as a single peak corresponding to a 1:1:1 stoichiometry (unpublished data).

### The CRB-3/PATJ/PALS polarity complex requires MALS-3

We next asked whether loss of MALS-3 affects the apico-basal polarization of its interaction partners. PALS, PATJ, and CRB-3 are enriched at tight junctions of proximal tubule epithelia (Fig. 5, A–D). Consistent with Western blotting results, PALS and PATJ staining is lost from tight junctions in *MALS-3*$^{\square/\square}$ (Fig. 5, A, B, and D); CRB-3 staining is reduced, and the remaining protein concentrates abnormally in punctate vesicles in the subapical region (Fig. 5, C and D). These major defects are not observed in collecting duct. In collecting duct epithelia, PALS and PATJ staining is reduced, but not lost, at the tight junction of the knockout, and CRB-3 localization appears normal (Fig. S3, A–D; available at http://www.jcb.org/cgi/content/full/jcb.200702054/DC1). Molecular compensation does not account for the localization of the CRB complex in *MALS-3*$^{\square/\square}$ collecting duct epithelia, as MALS-1 and - 2 are not detected (Fig. S3 E).

Loss of MALS-3 speciAcally disrupts the CRB complex. In proximal tubule and collecting duct epithelia, aPKC□, PAR-3, and ZO-1 remain at the tight junction (Fig. S3 H, Fig. S4, A, B, and D; and unpublished data). Other junction-associated proteins are also unaltered in renal epithelia from *MALS-3*$^{\square/\square}$ (Fig. S4, E and F).

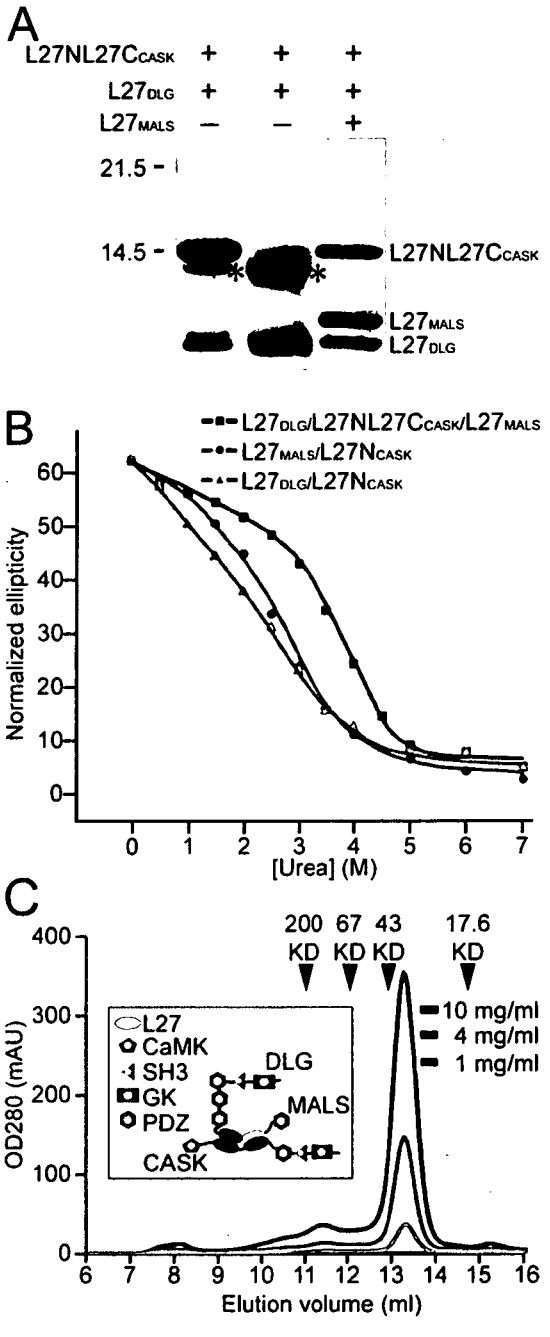


Figure 4. **The L27 domain of MALS mediates cooperative formation of a stable MALS/CASK/DLG ternary complex.** (A) Purification of a recombinant binary complex containing the single L27 domain of DLG and the tandem L27 domains of CASK shows degradation (asterisk, lane 1) and further degrades over 24 h at 4□C (asterisk, lane 2). Co-expression of MALS L27 domain stabilizes the MALS/CASK/DLG complex (lane 3), which does not degrade after 3 d at 35□C. (B) Comparison of the urea-induced denaturation profile of the $L27_{DLG}/L27NL27C_{CASK}/L27_{MALS}$ complex with those of the $(L27_{MALS}/L27C_{CASK})_2$ and $(L27N_{CASK}/L27_{DLG})_2$ complexes. The ellipticities of each spectrum at 222 nm were used to construct the denaturation curves. The MALS/CASK/DLG ternary complex is more stable than the two binary L27 domain complexes. (C) The tandem L27 domains of CASK assemble MALS and DLG into a stable 1:1:1 MALS/CASK/DLG ternary complex with a molecular mass of □ 38 kD over a wide concentration range. Cartoon inset shows stoichiometry and molecular oligomerization of the MALS/CASK/DLG complex.

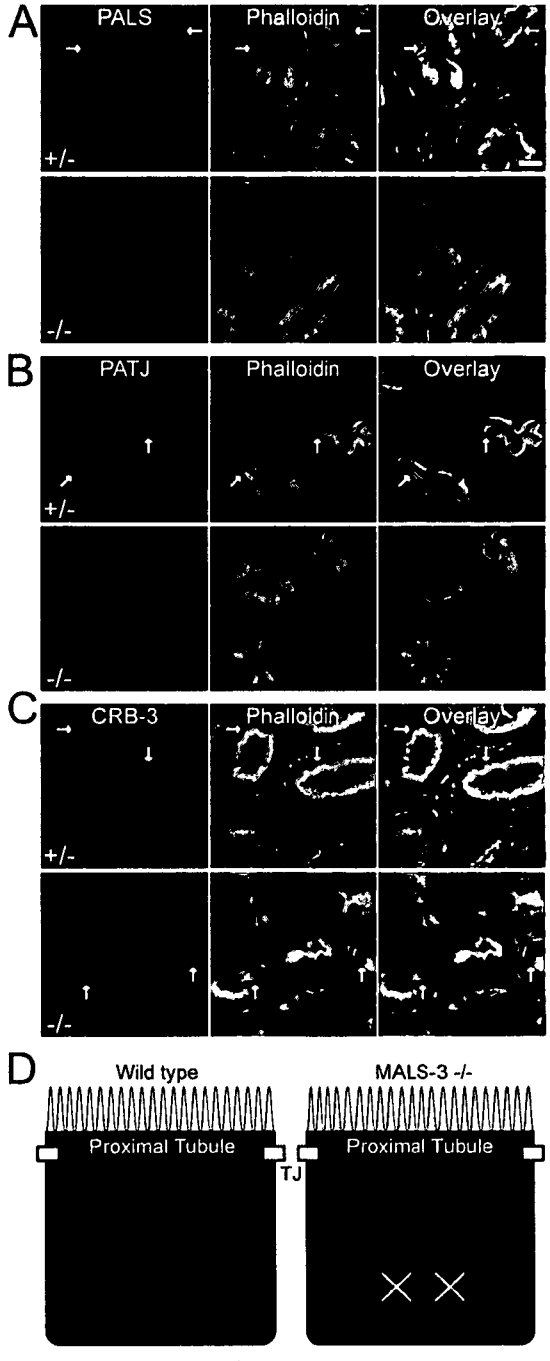


Figure 5. **Disruption of the PALS/PATJ/CRB-3 polarity complex in renal epithelia lacking MALS-3.** In 6-wk-old *MALS-3*$^{\Delta/\Delta}$ mice, PALS (A, top), PATJ (B, top), and CRB-3 (C, top) localize to the tight junction (arrows) below the apical brush border (phalloidin, green) of proximal tubule epithelia. In *MALS-3*$^{\Delta/\Delta}$ mice, PALS (A, bottom) and PATJ (B, bottom) are no longer detected in proximal tubules. Most proximal tubules in *MALS-3*$^{\Delta/\Delta}$ mice also lack CRB-3 (C, bottom), but some show a sub-apical punctate pattern, reminiscent of apical endosomes (arrows). (D) Cartoon summarizing the localization of the PALS/PATJ/CRB-3 complex (red) in wild-type proximal tubules (left) and the disruption of the complex in proximal tubule epithelia lacking MALS-3 (right). Bar ⊠ 10 ⊠m.

### MALS-3 mediates apical repulsion of DLG

The distribution DLG undergoes complex changes in *MALS-3*$^{\Delta/\Delta}$ (Fig. 6). Normally, DLG is predominantly distributed basolaterally in proximal tubule epithelia (Fig. 6, A, C, and D) and in more distal tubular segments of the nephron (Fig. 6, A and B; Fig. S3 F). Weaker tight junction and cytoplasmic staining is also observed in control animals (Fig. 6 C). In *MALS-3*$^{\Delta/\Delta}$, DLG is lost from the basolateral surface and becomes abnormally concentrated at tight junctions of epithelia in proximal tubules (Fig. 6, A, C, and D; and Fig. S2 B) and in more distal tubules (Fig. 6, A and B; Fig. S3 F). Other basolateral polarity proteins, scribble and LGL, remain concentrated along the basolateral membrane (Fig. S4 C, Fig. S3 G; and unpublished data).

### Kidney organogenesis in *MALS-3*$^{\Delta/\Delta}$

The resemblance of the *MALS-3* null phenotype to human nephronophthisis raises the possibility that MALS-3 may be involved in a common pathway with the six known nephronophthisis genes (NPHP1–6), which affect the organization and/or development of primary cilia (Torres et al., 2007). Consistent with this idea, CRB-3 localizes to cilia and *C. elegans* lacking *crb2b*, a CRB-3 homologue, exhibit renal hypoplasia, cysts, and tubular dilatation. Renal abnormalities in *crb2b* mutants are associated with malformation and dysfunction of primary cilia (Omori and Malicki, 2006). A conserved role for CRB-3 in cilia formation in mammalian epithelia has been demonstrated (Fan et al., 2004). Although CRB-3 is lost from the tight junction in renal epithelia lacking MALS-3, we found that CRB-3 localizes properly to primary cilia (Fig. 7 B), suggesting an alternative mechanism for targeting CRB-3 to cilia. Consistent with this hypothesis, PALS and PATJ are not detected in cilia (unpublished data) and the morphology of primary cilia appears unaltered in *MALS-3*$^{\Delta/\Delta}$ mice (Fig. 7 A). Analysis of EST databases (http://www.ncbi.nlm.nih.gov) revealed an alternatively spliced variant of CRB-3 (Fig. 7 C). The resulting protein product, CRB-3b, shares identical extracellular and transmembrane domains with canonical CRB-3, but has a divergent cytoplasmic tail. Importantly, the splicing variant results in a longer C-terminal tail that lacks the PDZ ligand (Fig. 7 C) required for PALS/PATJ interaction (Bhat et al., 1999; Roh et al., 2002). Interestingly, the CRB-3 antibody recognizes a doublet in kidney homogenates, with the larger product, likely CRB-3b, being more moderately reduced in *MALS-3*$^{\Delta/\Delta}$ (Fig. 3 C). Normalcy of ciliary structure and CRB localization do not exclude that more speciAc aspects of ciliary function are compromised in these animals (Hildebrandt and Zhou, 2007).

Dysfunction of primary cilia and associated centrosomes can impair cell proliferation (Simons and Walz, 2006) and thereby reduce kidney size in *MALS-3* mutants. To determine whether cell proliferation is altered in *MALS-3*$^{\Delta/\Delta}$ mice, mitotic cells in kidneys from E14.5 embryos were labeled using anti-phosphohistone3 antibody. We found no difference in cell proliferation between *MALS-3*$^{\Delta/\Delta}$ (0.388 ⊠ 0.013) and *MALS-3*$^{\Delta/\Delta}$ (0.375 ⊠ 0.013; P ⊠ 0.61) littermates (Fig. 8, A and B), excluding reduced cell division as the cause for the smaller kidney size.

Next, we examined whether changes in apoptosis/cell death contribute to this phenotype. Apoptotic cells are found in nephrogenic regions (Koseki et al., 1992) of E14.5 kidneys from both control and *MALS-3*$^{\Delta/\Delta}$ littermates (Fig. 8 C). However, abnormal cell death was detected in cells underlying the renal capsule in *MALS-3*$^{\Delta/\Delta}$ kidneys (Fig. 8, C and D), resulting in a

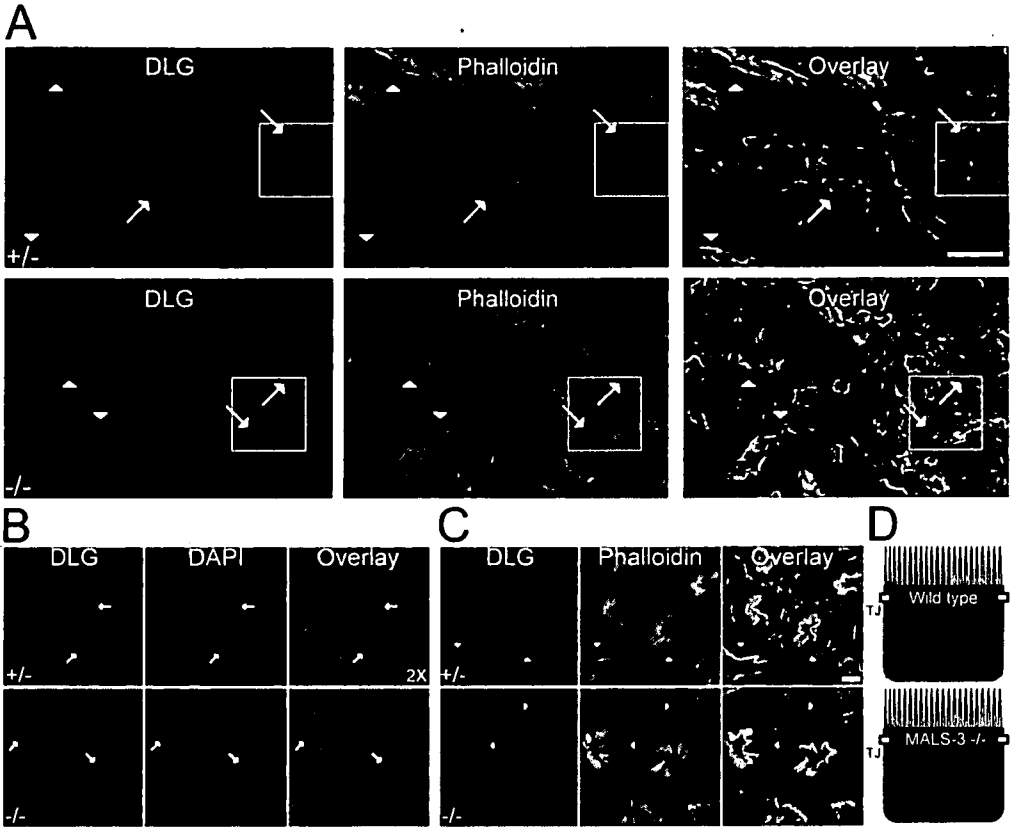


Figure 6. **DLG mislocalizes to the tight junction in renal epithelia lacking MALS-3.** (A, top) At the medullary boundary of a *MALS*$^{\Delta/\Delta}$ kidney, DLG strongly labels the basolateral membranes of tubules (arrows) and faintly stains the tight junction of proximal tubule segments (arrowheads). Proximal tubule brush border is stained with phalloidin (green). (A, bottom) Basolateral localization of DLG is lost in renal epithelia lacking MALS-3 (arrows and arrowheads, as above) and replaced by staining at the tight junction. (B, top) Higher magnification of A shows basolateral localization of DLG (arrows). (B, bottom) Epithelia lacking MALS-3 show specific loss of DLG at the basolateral membrane and accumulation of DLG at the tight junction. (C, top) High magnification images of proximal tubules in the cortex show basolateral (arrowheads) and tight junction staining for DLG. (C, bottom) Proximal tubules of *MALS-3*$^{\Delta/\Delta}$ mice have a discrete loss of DLG from the basolateral membrane (arrowheads). (D) Cartoon summarizing the localization of DLG (red) in control renal epithelia and epithelia lacking MALS-3. Bar □ 50 □m in A and 10 □m in C.

10-fold increase in apoptotic signal from *MALS-3*$^{\Delta/\Delta}$ (5.80 □ 0.76) as compared with *MALS-3*$^{\Delta/\Delta}$ kidneys (0.42 □ 0.19; P□ 0.007). These changes are detected as early as E12.5 (unpublished data), indicating that increased apoptosis causes reduced kidney size in *MALS-3*$^{\Delta/\Delta}$ mice.

### MALS-3 polarizes epithelia derived from the metanephric mesenchyme

The profound disruption of the CRB-3 complex in proximal tubule cells and the normalcy of PALS and CRB-3 localization in the collecting duct suggest that MALS-3 serves distinct functions in these two epithelial cell types. Proximal tubule and collecting duct cells derive from different tissue types (Dressler, 2006). During embryonic development, the ureteric bud extends from the WolfAan duct, invades the metanephric mesenchyme, and induces mesenchymal to epithelial cell transition. Tubules derived from metanephric mesenchyme extend from the glomerulus to the distal tubule, whereas the collecting duct derives from the ureteric bud (Fig. 9 A).

To assess the role of MALS-3 in each of these embryonic tissues, a new *MALS-3 □oxed* allele was created (Fig. S5, A–C, available at http://www.jcb.org/cgi/content/full/jcb.200702054/DC1). Breeding these *MALS-3 flox/flox* mice to transgenics that express cre recombinase under the control of the HoxB7 or Pax3 promoter (Fig. 9 B) allows deletion of *MALS-3* speciAcally from ureteric bud (*MALS-3 □ox/□ox; HoxB7-Pro-cre*) [UBKO] (Yu et al., 2002) or metanephric mesenchyme (*MALS-3 □ox/□ox; Pax3-Pro-cre*) [MMKO] (Li et al., 2000; Chang et al., 2004) (Fig. S5, D–F).

Levels of MALS-3 are differentially reduced in UBKO and MMKO mice (Fig. 9 C; Fig. S5, D–F). Importantly, gross abnormalities in kidney structure are only noted in the MMKO mice. Kidneys from MMKO mice are reduced in size (Fig. 9 D) with renal pathologies identical to *MALS-3*$^{\Delta/\Delta}$ mice (Fig. 9 E). These abnormalities are not observed in the UBKO mice (Fig. 9, D and E). Finally, in MMKO proximal tubules, but not UBKO, the CRB-3 and DLG complexes are affected (Fig. 9 F and unpublished data) in a manner similar to *MALS-3*$^{\Delta/\Delta}$.

### Kidney organogenesis in MMKO

Kidneys from adult MMKO mice phenocopy those of *MALS-3*$^{\Delta/\Delta}$ mice, indicating a shared developmental defect. Like the *MALS-3*$^{\Delta/\Delta}$, kidneys from MMKO embryos (E14.5) show extensive apoptosis underlying the renal capsule (Fig. 10 A).

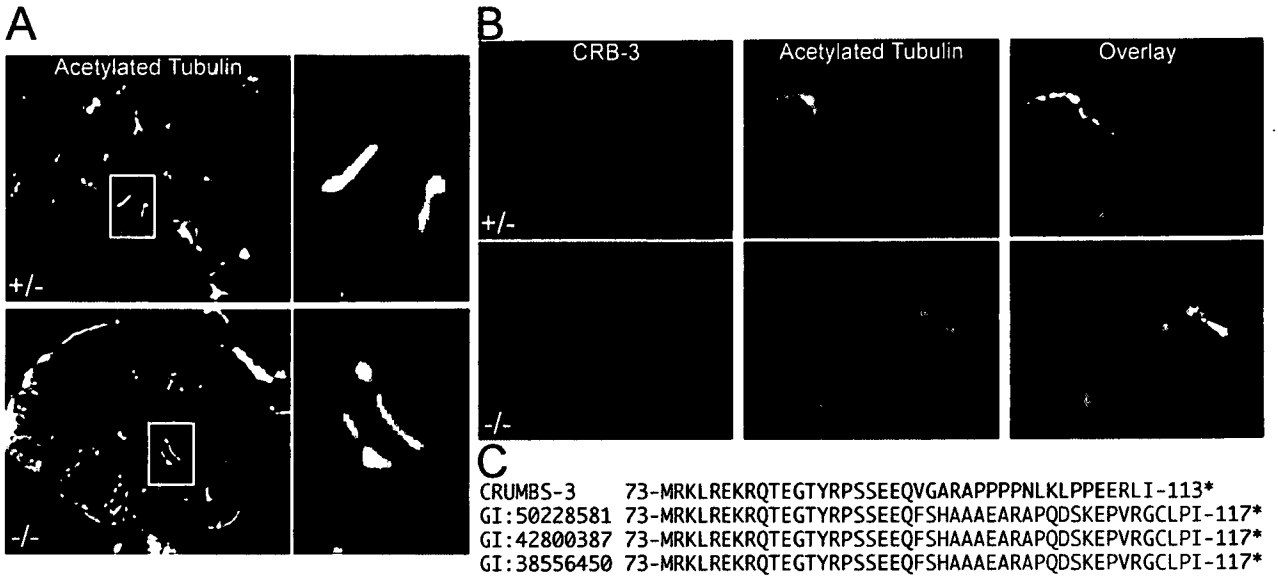


Figure 7. **Cilia show no changes in structure or localization for CRB-3.** (A) Cilia were visualized using anti-acetylated tubulin antibody. No obvious changes in cilia morphology were observed between control and *MALS-3*$^{\beta/\beta}$ kidneys. (B) CRB-3 (red) localizes to cilia in both control and *MALS-3*$^{\beta/\beta}$ kidneys. (C) Alignment of the intracellular portion of the translated protein sequences of canonical CRB-3 with three predicted protein sequences from the EST database. Underlined is the PDZ ligand in CRB-3 that is required for PALS/PATJ association; italicized are differences in the alternatively spliced C termini.

To determine whether defects in the CRB-3 and DLG polarity complexes underlie these developmental abnormalities, we examined the expression levels of these protein complexes in kidneys from MMKO embryos. Western blotting showed that both the CRB and DLG complexes were dramatically reduced (Fig. 10 B). These results show that MALS-3 is a critical component of the CRB and DLG complexes and that disruption of these complexes in the metanephric mesenchyme is associated with the renal defects in *MALS-3*$^{\beta/\beta}$ mice.

## Discussion

This study shows that MALS-3 is essential for polarization of renal epithelia and for kidney development. Kidneys from

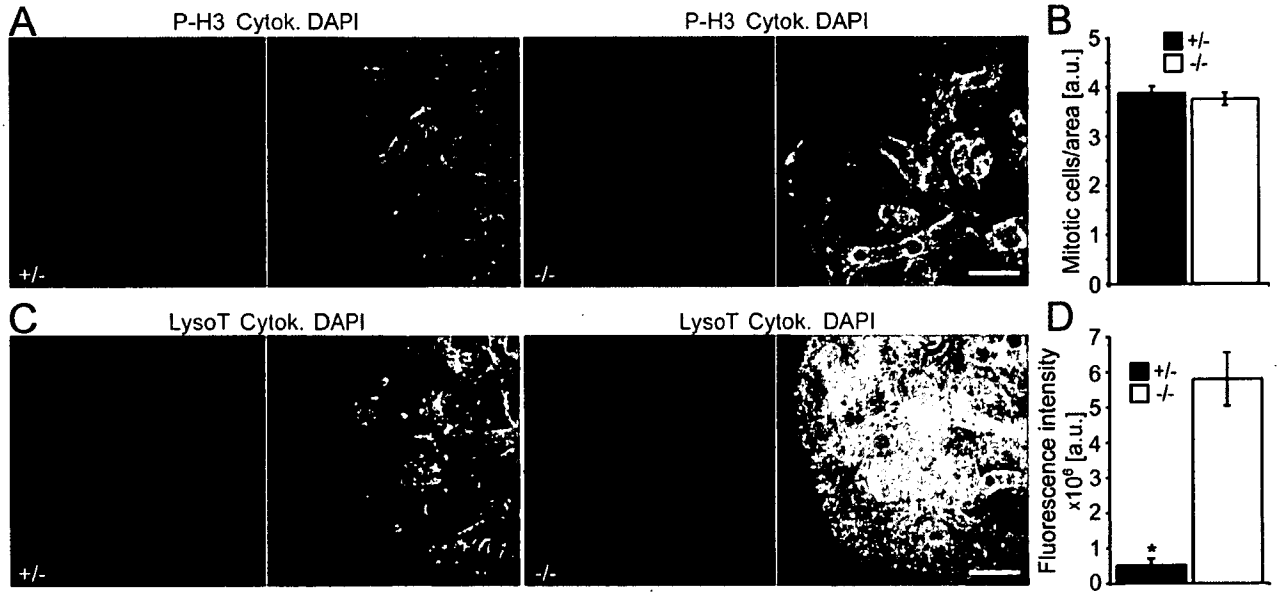


Figure 8. **Increased apoptosis in developing kidney of *MALS-3*$^{\beta/\beta}$.** (A) Kidneys from E14.5 embryos were stained with anti-phospho-histone3 antibody (red) to visualize cells in mitosis and counterstained with cytokeratin (green) and DAPI (blue). No changes in cell proliferation were observed between *MALS-3*$^{\beta/\beta}$ and *MALS-3*$^{\beta/\beta}$ kidneys. (B) Quantification of the number of mitotic cells. (C) Lysotracker (red) was used to label apoptotic cells and counterstained with cytokeratin (green) and DAPI (blue) in embryonic kidneys (E14.5). *MALS-3*$^{\beta/\beta}$ kidneys showed a dramatic increase in the number of apoptotic cells. (D) Quantification of Lysotracker fluorescence intensity from kidneys. Bar 100 μm.

*MALS-3*$^{\Delta/\Delta}$ mice display tubule dysgenesis, interstitial fibrosis, and cysts. These pathologies arise from defective polarization of tubule epithelia derived from the metanephric mesenchyme. MALS-3 mediates polarization of tubular epithelia through interactions with the CRB and DLG polarity complexes. Loss of MALS-3 disrupts polarized expression of these two critical protein complexes, establishing MALS-3 as an essential component of each. Furthermore, these data demonstrate that primary abnormalities in epithelial polarization can cause renal dysgenesis, fibrosis, and cysts.

### MALS-3 is a component of epithelial CRB-3 and DLG polarity complexes

*LIN-7* was originally identified in *C. elegans* as a gene essential for vulval development (Simske et al., 1996). In vulval precursor cells, LIN-7 is one component of a heterotrimeric PDZ protein complex that includes LIN-2 and LIN-10 (Kaech et al., 1998). Assembly of the complex is mediated through LIN-2, which binds LIN-7 through their complementary L27 domains, and binds LIN-10 through a more N-terminal site (Kaech et al., 1998). Vulval development requires signaling by an EGF-like receptor (LET-23) that binds the PDZ domain of LIN-7 (Simske et al., 1996). The LIN-2/-7/-10 complex localizes LET-23 to the basolateral surface where it binds its ligand (Kaech et al., 1998). Mutations in *lin-2*, *-7*, or *-10* mislocalize LET-23 to the apical domain and block vulval induction.

The LIN-2 (CASK)/LIN-7 (MALS)/LIN-10 (MINT-1) complex is conserved in mammalian brain, where it occurs both pre- and post-synaptically (Butz et al., 1998; Borg et al., 1999; Jo et al., 1999). Presynaptically, CASK binds to liprin-αs (Olsen et al., 2005a). Postsynaptically, the PDZ domain of MALS binds to the C-terminal tail of NMDA receptors (Jo et al., 1999). Altered neurotransmitter release in neurons lacking MALS is consistent with the MALS complex organizing the presynaptic active zone and vesicle cycling (Olsen et al., 2005a). Composition of the MALS complex in kidney differs fundamentally from that in *C. elegans* or brain, as kidney epithelium lacks MINT-1 (Okamoto and Sudhof, 1997). MINT-3 occurs in kidney, but it lacks the CASK interaction domain (Okamoto and Sudhof, 1997). MINT or liprin-α isoforms were not detected in MALS complexes isolated from kidney (Fig. 3).

Our work shows that MALS-3 occurs in two conserved epithelial cell polarity complexes and differentially colocalizes with these complexes in specific renal cell populations. In proximal tubule epithelia, MALS localizes to the tight junction—likely owing to its association with the CRB complex. *crb* was the first epithelial polarity gene characterized in *Drosophila* (Tepass et al., 1990). It is a transmembrane protein whose C-terminal tail interacts with the PDZ domain of stardust, SDT (PALS) (Roh et al., 2002), or dPATJ (PATJ) (Bhat et al., 1999). SDT is a membrane-associated guanylate kinase (MAGUK) that contains two L27 protein motifs (Kamberov et al., 2000). The first and second L27 domains of SDT bind to the L27 domains of dPATJ (Roh et al., 2002) and MALS (Kamberov et al., 2000), respectively.

Additionally, MALS associates with the basolateral DLG complex. In invertebrates, DLG mediates apico-basal polarization of epithelia and controls imaginal disc proliferation (Woods and Bryant, 1991). DLG is a MAGUK containing a single L27 domain that binds to the first of two L27 domains in CASK

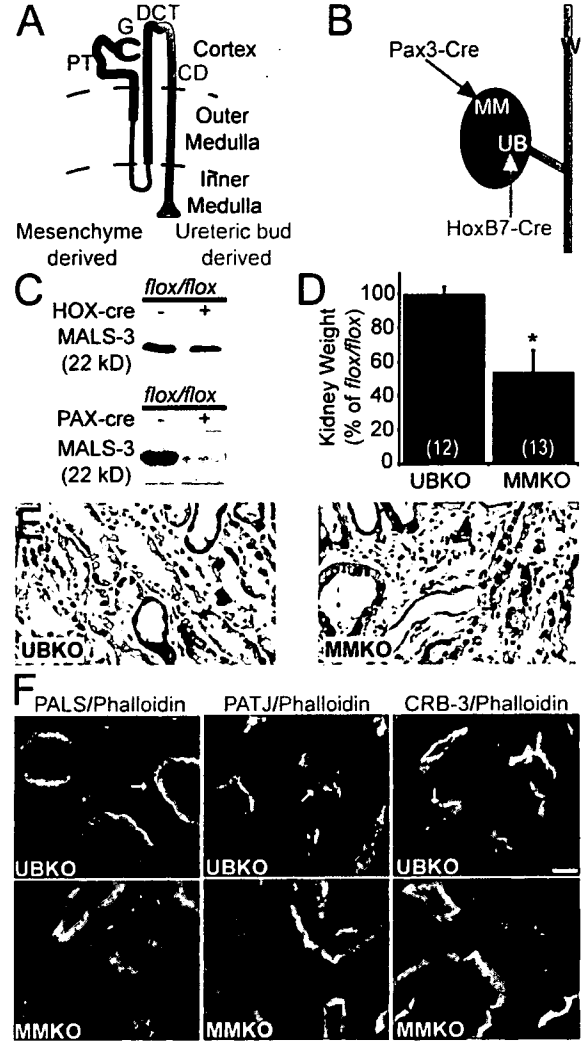


Figure 9. **Defective polarity cues in renal mesenchyme lacking MALS-3.** (A) Cartoon shows nephron segments and their embryonic origins. Abbreviations are as in Fig. 2 A. (B) Cartoon shows the expression of cre recombinase (cre) driven by *Pax3* promoter (*Pax3-cre*; blue) or *HoxB7* promoter (*HoxB7-cre*; orange). MM, metanephric mesenchyme; UB, ureteric bud; W, Wolfian duct. (C) Western blotting of adult kidney homogenates from *flox/flox* mice shows differential loss of MALS-3 in mice expressing cre from the *HoxB7* (Hox-cre) and *Pax3* (Pax-cre) promoters. (D) Elimination of MALS-3 from the metanephric mesenchyme fully reproduces the *MALS-3*$^{\Delta/\Delta}$ kidney deficiencies. *MALS-3 flox/flox; Pax3-Pro-cre* (MMKO) mice have kidneys that are reduced in magnitude to similar extent as *MALS-3*$^{\Delta/\Delta}$ mice (54.7% ± 13.3; $P < 0.01$). In contrast, kidneys from *MALS-3 flox/flox; HoxB7-Pro-cre* (UBKO) mice have kidneys similar in size (99.7% ± 4.6) to littermate controls. (E) Trichome-stained kidney section from a 6-wk-old UBKO mouse shows normal renal anatomy (left), whereas kidney from a MMKO mouse (right) shares anatomical abnormalities with *MALS-3*$^{\Delta/\Delta}$ mice, including tubular dilatation and fibrosis (arrow). (F) Immunohistochemistry from the cortex of kidneys from 6-wk-old UBKO and MMKO mice stained with phalloidin (green) to identify proximal tubule brush borders and DAPI (blue) for nuclei. PALS, PATJ, and CRB-3 all properly localize to the tight junction (arrows) of epithelia in proximal tubules of a kidney from UBKO mouse (F, top). In contrast, PALS, PATJ, and CRB-3 are lost from tight junction in proximal tubules from a MMKO mouse (F, bottom). Asterisk marks apical localization of CRB-3 in collecting duct.

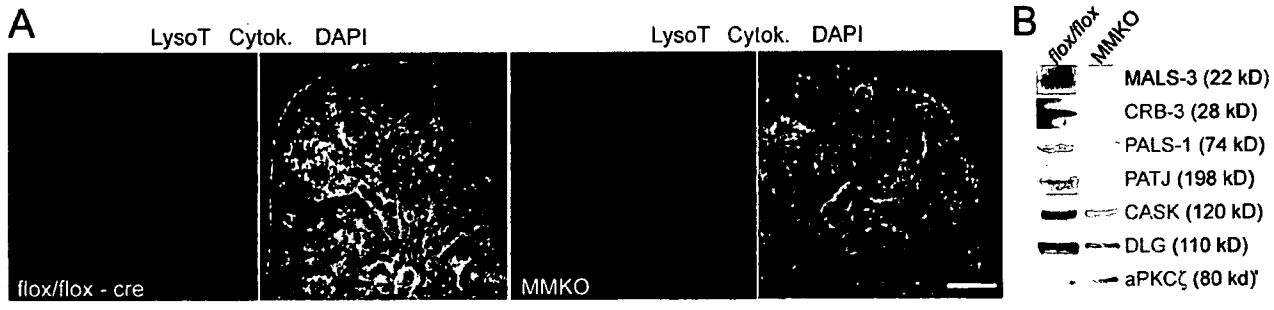


Figure 10. **Increased apoptosis associated with disrupted polarity complexes in developing kidney of MMKO.** (A) Apoptotic cells were visualized in embryonic kidneys (E14.5) with Lysotracker (red). Cytokeratin (green) and DAPI (blue) label epithelia and nuclei, respectively. As compared with control littermates, MMKO kidneys showed a dramatic increase in the number of apoptotic cells. Bar 100 m. (B) Kidney homogenates from *flox/flox* and MMKO mice immunoblotted for proteins of the CRB-3 and DLG polarity complexes show reduced expression of both complexes in MMKO embryonic kidneys.

(Lee et al., 2002), whose second L27 domain interacts with MALS (Straight et al., 2000). Other than CRB, all of these polarity proteins contain PDZ domains, whose binding surfaces are largely uninvolved in assembly of these protein complexes and may recruit additional components. MALS is the only known protein that functions as a core component of both the CRB and DLG complexes, positioning MALS as a central regulator of these complexes and cell polarity.

L27 domain interactions mediate assembly of MALS with the CRB and DLG complexes. Recently, the L27 domain structures of the DLG/CASK and PALS/PATJ complexes were independently determined by NMR and X-ray crystallography (Feng et al., 2004; Li et al., 2004). Each L27 domain comprises three -helices, and heterodimers form from a four-helical bundle of the Arst two helices. In the NMR structure of DLG/CASK, the third helix of each L27 formed another four helical bundles, assembling a tetramer (Feng et al., 2004). In contrast, X-ray structure showed only the hydrophobic residues of the PATJ L27 domains were necessary for assembling the PALS/PATJ tetramer (Li et al., 2004). Additional NMR studies showed that PALS/PATJ forms a tetrameric structure that resembles CASK/DLG and uses the C-terminal half of the third -helix of all four L27 domains (Feng et al., 2005).

These structural studies used two isolated L27 domains. However, many proteins, including CASK and PALS, have tandem L27 domains. We show that stability of tandem L27 structure requires occupation of both domains, which results in the formation of ternary complexes containing MALS/CASK/DLG or MALS/PALS/PATJ with a 1:1:1 stoichiometry. In each complex, four different L27 domains form a cooperative tetrameric complex. Presumably, the third -helices in the L27 domains interact between tandem L27 pairs, imparting stability and blocking formation of higher order oligomers. Future structural analyses will determine precise assembly mechanisms for these ternary complexes. Most importantly, these data reveal a mechanism for assembly of the CRB and DLG complexes and explain their dissolution in *MALS-3*$^{-/-}$ mice.

### MALS polarizes the apical CRB and basolateral DLG complexes

Loss of the CRB complex from proximal tubule tight junctions in MALS-3 mutants suggests that MALS-3, through its interaction with PALS (Kamberov et al., 2000), assembles the tight junction complex. Our results are supported by studies in MDCK cells that show MALS-3 knockdown disrupts the localization of PALS and PATJ (Straight et al., 2006). The current study makes several important advances on the role of MALS-3 in regulation of the CRB-3 complex. First, we show that the loss of PALS and PATJ in proximal tubule epithelia lacking MALS-3 is accompanied by a speciAc loss of CRB-3 from the tight junction. Importantly, these changes are not conserved in collecting duct epithelia, from which MDCK cells derive. This may explain why previous studies of MALS in MDCK cells have not described changes in CRB-3 expression, localization, or function (Straight et al., 2006). We also show that disruption of the CRB-3 complex results from the instability of the unbound PALS L27C domain, but direct interactions between MALS-3 and PATJ or CRB-3 cannot be ruled out. Finally, we show that CRB-3 properly localizes to cilia in these MALS-3–deAcient epithelia. An alternatively spliced CRB-3 variant, CRB-3b that lacks the PDZ ligand, likely accounts for these discrete localizations at the tight junction and cilia.

In addition to regulating assembly of the CRB complex, MALS-3 directs basolateral localization of DLG. The molecular mechanism underlying DLG mislocalization remains uncertain. MALS-3 associates with DLG through the MAGUK scaffolding protein CASK (Lee et al., 2002; Leonoudakis et al., 2004), suggesting that MALS-3 may directly control basolateral expression of DLG. In support of this, DLG and CASK coimmunoprecipitate with MALS-3 from kidney homogenates. Alternatively, DLG/LGL complexes that cross the apico-basal boundary may be recruited to aPKC by MALS-3. This recruitment may result in phosphorylation of LGL and restriction of the DLG/LGL complex to the basolateral membrane. Alternatively, the CRB complex may be required to apically exclude DLG. Fitting with this model, overexpression of CRB can rescue DLG polarization in *C. elegans* (Segbert et al., 2004).

### Polarity defects in *MALS-3* are restricted to specific renal epithelia

Why does MALS-3 differentially polarize in distinct epithelial cell populations? In proximal tubule epithelia derived from metanephric mesenchyme, MALS-3 is expressed at the tight junction and basolateral membrane, whereas in cells derived

from ureteric bud, MALS-3 is exclusively detected along the basolateral membrane. In *Drosophila*, cell-speciAc mechanisms have been identiAed for the MALS homologue, DLIN-7 (Bachmann et al., 2004). Here, the PALS homologue (SDT) associates with DLIN-7 at epithelial junctions, whereas *Drosophila* DLG interacts with DLIN-7 at the neuromuscular junction (Bachmann et al., 2004). Ectopic expression of SDT or DLG mediates DLIN-7 delivery to epithelial and neuromuscular junctions, respectively. This suggested that junctional targeting of MALS is downstream of both SDT and DLG (Bachmann et al., 2004). Our results are not consistent with this model. Loss of MALS-3 in proximal tubule epithelia causes dissolution of the CRB complex and redistribution of DLG, demonstrating that MALS are not always downstream of either PALS or DLG. Instead, MALS may primarily determine polarization in speciAc cell populations. In such a model, the PDZ binding partner for MALS could serve as the tight junction anchor. IdentiAcation of physiological PDZ ligands for MALS may help understand its cell type–speciAc functions.

Does MALS determine polarity in tissues other than kidney? In *Drosophila* with mutations to components of the CRB complex, numerous ectodermally derived epithelia are disorganized and degenerated (Tepass et al., 2001). The viability and fertility of *MALS-3* knockout mice indicate that many epithelial cell populations develop and function properly without MALS-3. The additional MALS isoforms may serve redundant functions; indeed, MALS-deAcient mice die from respiratory failure (Olsen et al., 2005a). That these mice show grossly normal size and morphology (Olsen et al., 2005a) suggests that MALS are not essential for polarizing all cell populations. Future studies of MALS triple-knockout mice should help deAne which cell types require MALS for polarization and determine how other pathways compensate or work in parallel.

### Implications for renal development and disease

Our studies reveal that renal defects arise solely from a loss of MALS-3 in epithelia derived from metanephric mesenchyme. MALS-3 is also present in epithelial cells derived from ureteric bud (Olsen et al., 2005b), but restricted ablation of MALS-3 in the ureteric bud neither causes changes in renal morphology nor disrupts CRB-3 polarization. By contrast, loss of MALS-3 in the metanephric mesenchyme is sufAcient to recapitulate the renal pathologies observed in *MALS-3*$^{\Delta/\Delta}$ mice. Localization of MALS-3 to the tight junctions in renal epithelia of mesenchymal origin suggests that tight junction–associated MALS-3 underlies the renal defects observed in *MALS-3*$^{\Delta/\Delta}$.

Mesenchymal to epithelial transition (MET) is a critical process underlying the development of numerous organs, including the kidney. Differentiation of epithelia from mesenchyme requires the establishment cell polarity. In MMKO mice, polarization cues originating from CRB and DLG complexes are disrupted. This likely leads to changes in the efAcacy of epithelial cell polarization during MET, resulting in apoptosis and smaller kidneys in *MALS-3* mutants. However, most renal epithelia in *MALS-3*$^{\Delta/\Delta}$ show normal cytoarchitecture. This indicates that redundant or parallel pathways compensate, albeit incompletely, for loss of the CRB and DLG complexes. Further analysis of *MALS-3*$^{\Delta/\Delta}$ embryos will be useful for determining the developmental processes regulated by these polarity complexes.

The converse of MET may underlie renal tubule simpliAcation/dedifferentiation and Abrosis in MALS-3 mutants. Recent studies suggest that epithelial to mesenchymal transition (EMT) of tubule epithelia is a signiAcant source of disease-related Abroblasts (Kalluri and Neilson, 2003; J.M. Lee et al., 2006). A critical step in EMT is a loss of cell polarity. Because MALS-3 epithelia are improperly polarized, uncontrolled EMT could account for the dedifferentiated tubular epithelia and Abrosis in MALS-3 mutants. Alternatively, renal epithelia lacking MALS-3 may be increasingly susceptible to external cues, such as injury or in□ammation, which can trigger EMT (Kalluri and Neilson, 2003; J.M. Lee et al., 2006). As defects in epithelial polarization and associated MET/EMT play central roles in renal cysts and Abrosis, *MALS-3*$^{\Delta/\Delta}$ mice should provide an important new model for understanding and treating these common kidney diseases.

## Materials and methods

#### Antibodies

Isoform specific and pan antibodies against MALS-1, -2, and -3 were generated in rabbits as described previously (Misawa et al., 2001). Anti-SAP-97 antibody was generated in rabbit (Topinka and Bredt, 1998); for immunohistochemistry an anti-SAP-97 antibody from Morgan Sheng (Massachusetts Institute of Technology, Cambridge, MA) was used. Rabbit anti-JAMS-A and anti-claudin antibodies were purchased from Invitrogen. PALS, PATJ, and Crumbs-3 antibodies were gifts from Ben Margolis (University of Michigan, Ann Arbor, MI) and rabbit anti-LGL antibody was provided by Valeri Vasioukhin (Fred Hutchinson Cancer Research Center, Seattle, WA). Rabbit anti-PAX2 was from BAbCO. Goat anti-aquaporin-2 antibody and rabbit anti-aPKC□ were from Santa Cruz Biotechnology, Inc. Rabbit anti-PAR-3 and anti-phospho-histone3 antibodies were from Upstate Biotechnology and goat anti-scribble antibody was from GeneTex, Inc. Mouse anti-CASK, anti-ZO-2, anti-□-catenin, anti-E-cadherin, and anti-N-cadherin were all purchased from Transduction Laboratories. Alexa-conjugated Phalloidin and secondary antibodies were purchased from Molecular Probes and mouse anti-pancytokeratin was from Sigma-Aldrich.

#### Mouse lines

The following mouse lines were used in this study: STOCK Gt(ROSA)26-Sortm1(Smo/EYFP)Amc/J, STOCK Tg(HoxB7-cre)13Amc/J, 129S4/SvJaeSor-Gt(ROSA)26Sortm1(FLP1)Dym/J, C57BL/6, and 129/Sv were purchased from The Jackson Laboratory. Pax3-Pro-Cre mice were a gift from Jonathan Epstein (University of Pennsylvania, Philadelphia, PA). MALS-1, -2, and -3 have been described previously (Misawa et al., 2001; Olsen et al., 2005a). For characterization of mice lacking MALS-1 and -2, double-knockout mice were compared with wild-type mice of a similar age and genetic background. Generation of *MALS-3 flox* mice is described below.

#### Isolation of MALS-3 genomic DNA and construction of targeting vector

Isolation of MALS-3 genomic DNA (BAC clone, mCG15974) has been described previously (Olsen et al., 2005a). For construction of the targeting vector, a 1.9-kb region encoding the targeted exons (the fourth and fifth exon) of MALS-3 was PCR-amplified, digested with ClaI, and subcloned into the ClaI site of pks2loxPFRTNT (a gift from Shinya Yamanaka, Kyoto University, Kyoto, Japan). A 1-kb region downstream from the targeted exons was PCR-amplified, digested with BamHI and EcoRI, and subcloned into the BamHI-EcoRI sites of pks2loxPFRTNT. Finally, a 5.8-kb genomic region upstream to the targeted exons was PCR-amplified, digested with KpnI and BamHI, and inserted into the KpnI-SalI sites of the pks2loxPFRTNT vector. Two loxP sites flank targeted exons and a neomycin cassette. Two FRT sites flank the neomycin cassette for its removal.

#### Generation of *MALS-3 loxP* mice

The targeting vector was linearized and electroporated into R-1 ES cells. Clones resistant to G418 and gancyclovir were analyzed for recombination by PCR. To ensure proper homologous recombination, PCR-positive

clones were further analyzed by Southern blotting using probes containing genomic sequences outside of the targeting vector and with a neo probe. Properly targeted clones were injected into blastocysts from C57BL6 mice and transferred to surrogate mothers (Transgenic Facility, Stanford University, Stanford, CA). Male chimeras were mated with 129S4/SvJae-Sor-Gt(ROSA)26Sortm1(FLP1)Dym/J (The Jackson Laboratory) females for transmission of the mutated allele through the germ line and for removal of the neomycin cassette from the targeted allele. Genotypes for *MALS-3 loxP* mice lacking the neomycin cassette were determined by Southern blotting or by PCR using the primers: 5′-GAAAATGCTTCTGTCCGTTTGC-3′ and 5′-ATTGCTGTCACTTGGTCGTGGC-3′ which yields a 280-bp product for the wild-type allele and a 350-bp product for the targeted allele. Presence of the cre-recombinase and EYFP transgenes was determined using the following primer pairs: 5′-GAAAATGCTTCTGTCCGTTTGC-3′ and 5′-ATTGCTGTCACTTGGTCTGGC-3′ for cre and 5′-CCCTGAAGTTCATCTGCACCACC-3′ and 5′-GGACTTGTACAGCTCGTCCATGCC-3′ for EYFP.

**Protein expression and purification**

Genes corresponding to the L27 domain of rat DLG ($L27_{DLG}$, residues 1–65), the L27 domain of mouse MALS ($L27_{MALS}$, residues 2–78), and the tandem L27 domain of rat CASK (L27NL27C$_{CASK}$, residues 329–460) were PCR amplified from the respective full-length cDNAs. The single-chain fusion protein, containing $L27_{DLG}$, L27NL27C$_{CASK}$, and $L27_{MALS}$ connected with a thrombin-cleavable segment (Leu-Val-Pro-Arg-Gly-Ser-Ser-Gly), was cloned into a modified version of the pET32a vector in which the S-tag and the thrombin recognition site were replaced by a sequence encoding a protease 3C cleavage site (Leu-Glu-Val-Leu-Phe-Gln-Gly-Pro). Similarly, the single chain fusion protein, containing $L27_{DLG}$ and L27NL27C$_{CASK}$ connected with a thrombin-cleavable segment, was PCR-amplified and inserted into the modified pET32a vector. Bacterial cells harboring the fusion protein expression plasmid were grown at 37°C, and protein expression was induced by IPTG at the same temperature for 3 h. The His-tagged, thioredoxin-containing protein was purified under native conditions using Ni-NTA agarose (QIAGEN) affinity chromatography. After protease 3C digestion the N-terminal His-tag and thioredoxin were removed by passing the digestion mixture through an S-200 gel filtration column, then the single-chain protein was digested by thrombin and the L27 domain complex protein was further passed through the same size-exclusion column. The expression and purification of $L27_{MALS}$/L27C$_{CASK}$ and L27N$_{CASK}$/$L27_{DLG}$ complex proteins were described previously (Feng et al., 2004, 2005).

**Kidney immunohistochemistry**

Adult mice were anesthetized and perfused with 2% paraformaldehyde in PBS. Kidneys were removed, immersed in the same fixative for 2 h at 4°C, and then cryoprotected in PBS containing 30% sucrose overnight at 4°C. Frozen sections (10 μm) were rehydrated with PBS containing 0.1% Triton X-100 (PBS-X) for 20 min and incubated for 1 h in blocking solution (PBS-X containing 1% BSA). Primary and secondary antibodies were diluted in blocking solution and incubated overnight at 4°C and 2 h at room temperature, respectively. Antibody incubations were followed by three washes in PBS-X. Sections were mounted with coverslips in Flouromount-G (Southern Biotechnology Associates, Inc.). Images were taken with a confocal microscope (LSM 5 Pascal Axioplan 2; Carl Zeiss MicroImaging, Inc.) under Zeiss 63× 1.4 or 40× 1.3 oil-immersion objectives or a Zeiss 10× 0.3 objective at room temperature and acquired using LSM 5 Pascal (v.3.2) software. Images were processed using Adobe Photoshop. To study primary molecular defects in *MALS-3*$^{-/-}$ mice, only kidneys that showed normal arrangement of tubules with mild anatomical abnormalities were used for localizing aPKC/Crumbs/DLG complexes. More than three sections from six KO and six control littermates were examined. Proximal tubules were identified by phalloidin staining of apical brush border, whereas collecting ducts were stained using aquaporin-2 antibody.

For hematoxylin and eosin or trichome staining, perfused kidneys were immersed in 4% paraformaldehyde in PBS overnight at 4°C, dehydrated using an alcohol series and xylene, and embedded in paraffin. Paraffin sections (4 μm) were cut on a microtome and mounted onto slides. All light images were taken using an AxioCam HRC camera mounted to a microscope (Eclipse E6600; Nikon) with10× 0.3 and 20× 0.5 objectives at room temperature. Images were acquired with AxioVision (v4.6) software and processed in Adobe Photoshop.

**Renal function**

Mice were housed in metabolic cages on a 12-h light-dark cycle and fed ad libitum on normal chow. After 24 h, urine was collected under oil, animals were anesthetized with Inactin (100 mg/kg, i.p.), and blood was collected by cardiac puncture. Blood and urine chemistries were measured by automated methods (IDEXX, West Sacramento, CA). For measurements of urine diluting and concentrating ability, urine osmolarity was measured using a vapor pressure osmometer (Wescor) after animals were fed a high water content diet (Bouby et al., 1990, 1996) for 48 h and then again after mice (12 h) were injected with deamino-Cys, D-Arg9-vasopressin (DDAVP, 1 μg/Kg, i.p.) and feeding water was withdrawn.

**Immunoprecipitations**

Adult mouse kidneys from *MALS-3*$^{-/-}$ or *MALS-3*$^{+/+}$ mice were homogenized in three volumes of STE buffer (320 mM sucrose, 20 mM Tris, pH 7.4, and 2 mM EDTA) containing 10 μg/ml leupeptin, 10 μg/ml aprotinin and 200 μg/ml PMSF. Homogenates were centrifuged at 20,000 *g* for 1 h and pellets were resuspended in TET buffer (20 mM Tris, pH 8.0), 1 mM EDTA, and 1.3% Triton X-100) containing 10 μg/ml leupeptin, 10 μg/ml aprotinin, and 50 μg/ml PMSF. Lysates were pelleted at 100,000 *g* for 1 h. Precleared lysates were immunoprecipitated with 5 μg of MALS-3 antibody or control rabbit IgG overnight at 4°C. To collect immunoprecipitated protein complexes, 80 μl of a 50% protein A–Sepharose slurry was added to the lysates and incubated for 1 h at 4°C. Immunoprecipitates were washed extensively and loaded onto SDS-PAGE to separate the proteins. Gels were either silver stained or transferred to nitrocellulose for Western blotting.

**Nano-LC-ESI-Qq-TOF tandem mass spectrometry analysis**

Gel bands were reduced with 10 mM dithiothreitol (DTT) followed by alkylation with 55 mM iodoacetamide. Proteins were digested with trypsin and extracted with a 50% acetonitrile/5% formic acid solution. The peptides were dried down and resuspended in 0.1% formic acid then separated via HPLC using a 75 μM × 15 cm reverse-phase C-18 column (LC Packings) running a 3–32% acetonitrile gradient in 0.1% formic acid on an Agilent 1100 series HPLC. The LC eluent was coupled to a micro-ionspray source attached to a QSTAR Pulsar mass spectrometer (MDS Sciex). Peptides were analyzed in positive ion mode.

**Analytical gel filtration**

Size-exclusion chromatography was performed on an AKTA FPLC system using a Superose 12 10/30 column (GE Healthcare). Protein samples were dissolved in 100 mM potassium phosphate buffer containing 1 mM DTT. The column was calibrated with the low molecular mass column calibration kit from GE Healthcare.

**Urea denaturation**

Urea denaturation of L27 domain complexes was monitored by acquiring circular dichroism spectra of protein samples at each urea concentration. Data were collected on a JASCO J-720 spectropolarimeter at room temperature. The sample contained 15 μM protein in buffer (10 mM Tris-HCl, pH 7.5, 1 mM EDTA, and 1 mM DTT).

**Cell death and proliferation**

To detect dying cells, LysoTracker (Invitrogen) labeling of embryonic kidneys was performed as described previously (Grieshammer et al., 2005). In brief, isolated kidneys (six kidneys each for control and *MALS-3*$^{-/-}$) were incubated with 5 μl/ml LysoTracker solution in HBSS at 37°C for 30 min, rinsed in HBSS, fixed in 4% PFA in PBS, and stored at −20°C in 100% methanol. After rehydration into PBS, E14.5 kidneys were sectioned (100 μm), permeabilized in PBS contaning 0.1% Tween 20, and stained with anti-cytokeratin (Sigma-Aldrich). After extensive washing, cytokeratin antibody was detected using Alexa488-conjugated donkey anti–mouse antibody (Invitrogen) and nuclei were labeled with DAPI. All images were taken with a confocal microscope (LSM 5 Pascal Axioplan 2; Carl Zeiss MicroImaging, Inc.) under Zeiss 25× 0.8 objective (zoom setting 1 or 2) at room temperature and acquired using LSM 5 Pascal (v.3.2) software. Total fluorescent intensity was analyzed using MetaMorph software and images were processed using Adobe Photoshop. The average intensity of three individual optical sections from each stack was calculated. Five stacks of individual kidneys were analyzed for each condition. For apoptosis in E12.5 whole mounts, kidneys were rehydrated into PBS containing Tween 20 (0.1%) and counterstained with anti-PAX2 antibody. The rest of the staining procedure was performed as described above. To detect cells in mitosis, isolated kidneys (13 sections from 5 control kidneys and 14 from 5 *MALS-3*$^{-/-}$ kidneys) were fixed in 4% PFA, washed, sectioned (100 μm), and incubated with rabbit anti-phospho-histone H3 antibody (1:200; Upstate Biotechnology) and co-stained with anti-cytokeratin as above. Alexa546-conjugated donkey anti–rabbit antibody was used for labeling phospho-histone antibody. All images were obtained with a confocal microscope and >20 optical sections were analyzed for each kidney.

**Online supplemental material**

Figure S1 shows renal cysts in kidney sections from adult and embryonic *MALS-3*$^{-/-}$ mice as well as urine concentrating ability in mutant mice. Figure S2 shows the colocalization of MALS and DLG with the tight junction. Figure S3 shows partial disruption of polarity complexes in collecting ducts of *MALS-3*$^{-/-}$. Figure S4 shows that localization of PAR-3, aPKC, and SCRIB does not require MALS-3. Figure S5 depicts the generation and characterization of the *MALS-3 floxed* allele. Online supplemental material is available at http://www.jcb.org/cgi/content/full/jcb.200702054/DC1.

The authors wish to thank Uta Grieshammer for assisting with study of embryonic mice and Zoltan Laszik and Stephen Gluck for assisting with the renal pathology as well as Keith Mostov, Louis Reichardt, Michael Caplan, David Pearce, and Vivek Bhalla for their critical reading of the manuscript. The authors declare there is no financial conflict of interest related to this work.

This work was supported by grants from the National Institutes of Health (to D.S. Bredt and O. Olsen) and the Research Grant Council of Hong Kong (to M. Zhang).

Submitted: 8 February 2007
Accepted: 11 September 2007

## References

Bachmann, A., M. Schneider, E. Theilenberg, F. Grawe, and E. Knust. 2001. *Drosophila* Stardust is a partner of Crumbs in the control of epithelial cell polarity. *Nature.* 414:638–643.

Bachmann, A., M. Timmer, J. Sierralta, G. Pietrini, E.D. GundelAnger, E. Knust, and U. Thomas. 2004. Cell type-speciAc recruitment of *Drosophila* Lin-7 to distinct MAGUK-based protein complexes deAnes novel roles for Sdt and Dlg-S97. *J. Cell Sci.* 117:1899–1909.

Betschinger, J., K. Mechtler, and J.A. Knoblich. 2003. The Par complex directs asymmetric cell division by phosphorylating the cytoskeletal protein Lgl. *Nature.* 422:326–330.

Bhat, M.A., S. Izaddoost, Y. Lu, K.O. Cho, K.W. Choi, and H.J. Bellen. 1999. Discs Lost, a novel multi-PDZ domain protein, establishes and maintains epithelial polarity. *Cell.* 96:833–845.

Bilder, D., and N. Perrimon. 2000. Localization of apical epithelial determinants by the basolateral PDZ protein Scribble. *Nature.* 403:676–680.

Bilder, D., M. Li, and N. Perrimon. 2000. Cooperative regulation of cell polarity and growth by *Drosophila* tumor suppressors. *Science.* 289:113–116.

Borg, J.-P., M.O. Lõpez-Figueroa, M. de Taddèo-Borg, D.E. Kroon, R.S. Turner, S.J. Watson, and B. Ben Margolis. 1999. Molecular analysis of the X11-mLin-2/CASK complex in brain. *J. Neurosci.* 19:1307–1316.

Bouby, N., S. Bachmann, D. Bichet, and L. Bankir. 1990. Effect of water intake on the progression of chronic renal failure in the 5/6 nephrectomized rat. *Am. J. Physiol.* 258:F973–F979.

Bouby, N., M. Ahloulay, E. Nsegbe, M. Déchaux, F. Schmitt, and L. Bankir. 1996. Vasopressin increases glomerular Altration rate in conscious rats through its antidiuretic action. *J. Am. Soc. Nephrol.* 7:842–851.

Butz, S., M. Okamoto, and T.C. Sudhof. 1998. A tripartite protein complex with the potential to couple synaptic vesicle exocytosis to cell adhesion in brain. *Cell.* 94:773–782.

Campo, C., A. Mason, D. Maouyo, O. Olsen, D. Yoo, and P.A. Welling. 2005. Molecular mechanisms of membrane polarity in renal epithelial cells. *Rev. Physiol. Biochem. Pharmacol.* 153:47–99.

Chang, C.P., B.W. McDill, J.R. Neilson, H.E. Joist, J.A. Epstein, G.R. Crabtree, and F. Chen. 2004. Calcineurin is required in urinary tract mesenchyme for the development of the pyeloureteral peristaltic machinery. *J. Clin. Invest.* 113:1051–1058.

Djiane, A., S. Yogev, and M. Mlodzik. 2005. The apical determinants aPKC and dPatj regulate Frizzled-dependent planar cell polarity in the *Drosophila* eye. *Cell.* 121:621–631.

Dressler, G.R. 2006. The cellular basis of kidney development. *Annu. Rev. Cell Dev. Biol.* 22:509–529.

Etemad-Moghadam, B., S. Guo, and K.J. Kemphues. 1995. Asymmetrically distributed PAR-3 protein contributes to cell polarity and spindle alignment in early *C. elegans* embryos. *Cell.* 83:743–752.

Fan, S., T.W. Hurd, C.J. Liu, S.W. Straight, T. Weimbs, E.A. Hurd, S.E. Domino, and B. Margolis. 2004. Polarity proteins control ciliogenesis via kinesin motor interactions. *Curr. Biol.* 14:1451–1461.

Feng, W., J.F. Long, J.S. Fan, T. Suetake, and M. Zhang. 2004. The tetrameric L27 domain complex as an organization platform for supramolecular assemblies. *Nat. Struct. Mol. Biol.* 11:475–480.

Feng, W., J.F. Long, and M. Zhang. 2005. A uniAed assembly mode revealed by the structures of tetrameric L27 domain complexes formed by mLin-2/mLin-7 and Patj/Pals1 scaffold proteins. *Proc. Natl. Acad. Sci. USA.* 102:6861–6866.

Gateff, E., and H.A. Schneiderman. 1969. Neoplasms in mutant and cultured wild-tupe tissues of *Drosophila*. *Natl. Cancer Inst. Monogr.* 31:365–397.

Grieshammer, U., C. Cebrian, R. Ilagan, E. Meyers, D. Herzlinger, and G.R. Martin. 2005. FGF8 is required for cell survival at distinct stages of nephrogenesis and for regulation of gene expression in nascent nephrons. *Development.* 132:3847–3857.

Hildebrandt, F., and W. Zhou. 2007. Nephronophthisis-associated ciliopathies. *J. Am. Soc. Nephrol.* 18:1855–1871.

Hong, Y., B. Stronach, N. Perrimon, L.Y. Jan, and Y.N. Jan. 2001. *Drosophila* Stardust interacts with Crumbs to control polarity of epithelia but not neuroblasts. *Nature.* 414:634–638.

Hurd, T.W., L. Gao, M.H. Roh, I.G. Macara, and B. Margolis. 2003. Direct interaction of two polarity complexes implicated in epithelial tight junction assembly. *Nat. Cell Biol.* 5:137–142.

Izumi, Y., T. Hirose, Y. Tamai, S. Hirai, Y. Nagashima, T. Fujimoto, Y. Tabuse, K.J. Kemphues, and S. Ohno. 1998. An atypical PKC directly associates and colocalizes at the epithelial tight junction with ASIP, a mammalian homologue of *Caenorhabditis elegans* polarity protein PAR-3. *J. Cell Biol.* 143:95–106.

Jo, K., R. Derin, M. Li, and D.S. Bredt. 1999. Characterization of MALS/Velis-1, -2, and -3: a family of mammalian LIN-7 homologs enriched at brain synapses in association with the postsynaptic density-95/NMDA receptor postsynaptic complex. *J. Neurosci.* 19:4189–4199.

Joberty, G., C. Petersen, L. Gao, and I.G. Macara. 2000. The cell-polarity protein Par6 links Par3 and atypical protein kinase C to Cdc42. *Nat. Cell Biol.* 2:531–539.

Kaech, S.M., C.W. WhitAeld, and S.K. Kim. 1998. The LIN-2/LIN-7/LIN-10 complex mediates basolateral membrane localization of the *C. elegans* EGF receptor LET-23 in vulval epithelial cells. *Cell.* 94:761–771.

Kalluri, R., and E.G. Neilson. 2003. Epithelial-mesenchymal transition and its implications for Abrosis. *J. Clin. Invest.* 112:1776–1784.

Kamberov, E., O. Makarova, M. Roh, A. Liu, D. Karnak, S. Straight, and B. Margolis. 2000. Molecular cloning and characterization of Pals, proteins associated with mLin-7. *J. Biol. Chem.* 275:11425–11431.

Koseki, C., D. Herzlinger, and Q. al-Awqati. 1992. Apoptosis in metanephric development. *J. Cell Biol.* 119:1327–1333.

Lee, D.B., E. Huang, and H.J. Ward. 2006. Tight junction biology and kidney dysfunction. *Am. J. Physiol. Renal Physiol.* 290:F20–F34.

Lee, J.M., S. Dedhar, R. Kalluri, and E.W. Thompson. 2006. The epithelial-mesenchymal transition: new insights in signaling, development, and disease. *J. Cell Biol.* 172:973–981.

Lee, S., S. Fan, O. Makarova, S. Straight, and B. Margolis. 2002. A novel and conserved protein-protein interaction domain of mammalian Lin-2/CASK binds and recruits SAP97 to the lateral surface of epithelia. *Mol. Cell. Biol.* 22:1778–1791.

Leonoudakis, D., L.R. Conti, C.M. Radeke, L.M. McGuire, and C.A. Vandenberg. 2004. A multiprotein trafAcking complex composed of SAP97, CASK, Veli, and Mint1 is associated with inward rectiAer Kir2 potassium channels. *J. Biol. Chem.* 279:19051–19063.

Li, J., F. Chen, and J.A. Epstein. 2000. Neural crest expression of Cre recombinase directed by the proximal Pax3 promoter in transgenic mice. *Genesis.* 26:162–164.

Li, Y., D. Karnak, B. Demeler, B. Margolis, and A. Lavie. 2004. Structural basis for L27 domain-mediated assembly of signaling and cell polarity complexes. *EMBO J.* 23:2723–2733.

Lin, D., A.S. Edwards, J.P. Fawcett, G. Mbamalu, J.D. Scott, and T. Pawson. 2000. A mammalian PAR-3-PAR-6 complex implicated in Cdc42/Rac1 and aPKC signalling and cell polarity. *Nat. Cell Biol.* 2:540–547.

Medina, E., J. Williams, E. Klipfell, D. Zarnescu, G. Thomas, and A. Le Bivic. 2002. Crumbs interacts with moesin and beta(Heavy)-spectrin in the apical membrane skeleton of *Drosophila*. *J. Cell Biol.* 158:941–951.

Misawa, H., Y. Kawasaki, J. Mellor, N. Sweeney, K. Jo, R.A. Nicoll, and D.S. Bredt. 2001. Contrasting localizations of MALS/LIN-7 PDZ proteins in brain and molecular compensation in knockout mice. *J. Biol. Chem.* 276:9264–9272.

Okamoto, M., and T.C. Sudhof. 1997. Mints, Munc18-interacting proteins in synaptic vesicle exocytosis. *J. Biol. Chem.* 272:31459–31464.

Olsen, O., H. Liu, J.B. Wade, J. Merot, and P.A. Welling. 2002. Basolateral membrane expression of the Kir 2.3 channel is coordinated by PDZ interaction with Lin-7/CASK complex. *Am. J. Physiol. Cell Physiol.* 282:C183–C195.

Olsen, O., K.A. Moore, M. Fukata, T. Kazuta, J.C. Trinidad, F.W. Kauer, M. Streuli, H. Misawa, A.L. Burlingame, R.A. Nicoll, and D.S. Bredt. 2005a.

Neurotransmitter release regulated by a MALS-liprin-alpha presynaptic complex. *J. Cell Biol.* 170:1127–1134.

Olsen, O., J.B. Wade, N. Morin, D.S. Bredt, and P.A. Welling. 2005b. Differential localization of mammalian Lin-7 (MALS/Veli) PDZ proteins in the kidney. *Am. J. Physiol. Renal Physiol.* 288:F345–F352.

Omori, Y., and J. Malicki. 2006. *oko meduzy* and related crumbs genes are determinants of apical cell features in the vertebrate embryo. *Curr. Biol.* 16:945–957.

Perego, C., C. Vanoni, A. Villa, R. Longhi, S.M. Kaech, E. Frohli, A. Hajnal, S.K. Kim, and G. Pietrini. 1999. PDZ-mediated interactions retain the epithelial GABA transporter on the basolateral surface of polarized epithelial cells. *EMBO J.* 18:2384–2393.

Perego, C., C. Vanoni, S. Massari, R. Longhi, and G. Pietrini. 2000. Mammalian LIN-7 PDZ proteins associate with beta-catenin at the cell-cell junctions of epithelia and neurons. *EMBO J.* 19:3978–3989.

Plant, P.J., J.P. Fawcett, D.C. Lin, A.D. Holdorf, K. Binns, S. Kulkarni, and T. Pawson. 2003. A polarity complex of mPar-6 and atypical PKC binds, phosphorylates and regulates mammalian Lgl. *Nat. Cell Biol.* 5:301–308.

Roh, M.H., O. Makarova, C.J. Liu, K. Shin, S. Lee, S. Laurinec, M. Goyal, R. Wiggins, and B. Margolis. 2002. The Maguk protein, Pals1, functions as an adapter, linking mammalian homologues of Crumbs and Discs Lost. *J. Cell Biol.* 157:161–172.

Schneeberger, E.E., and R.D. Lynch. 1992. Structure, function, and regulation of cellular tight junctions. *Am. J. Physiol.* 262:L647–L661.

Segbert, C., K. Johnson, C. Theres, D. van Furden, and O. Bossinger. 2004. Molecular and functional analysis of apical junction formation in the gut epithelium of *Caenorhabditis elegans*. *Dev. Biol.* 266:17–26.

Shelly, M., Y. Mosesson, A. Citri, S. Lavi, Y. Zwang, N. Melamed-Book, B. Aroeti, and Y. Yarden. 2003. Polar expression of ErbB-2/HER2 in epithelia. Bimodal regulation by Lin-7. *Dev. Cell.* 5:475–486.

Shin, K., V.C. Fogg, and B. Margolis. 2006. Tight junctions and cell polarity. *Annu. Rev. Cell Dev. Biol.* 22:207–235.

Simons, M., and G. Walz. 2006. Polycystic kidney disease: cell division without a c(l)ue? *Kidney Int.* 70:854–864.

Simske, J.S., S.M. Kaech, S.A. Harp, and S.K. Kim. 1996. LET-23 receptor localization by the cell junction protein LIN-7 during *C. elegans* vulval induction. *Cell.* 85:195–204.

Straight, S.W., D. Karnak, J.P. Borg, E. Kamberov, H. Dare, B. Margolis, and J.B. Wade. 2000. mLin-7 is localized to the basolateral surface of renal epithelia via its NH(2) terminus. *Am. J. Physiol. Renal Physiol.* 278: F464–F475.

Straight, S.W., L. Chen, D. Karnak, and B. Margolis. 2001. Interaction with mLin-7 alters the targeting of endocytosed transmembrane proteins in mammalian epithelial cells. *Mol. Biol. Cell.* 12:1329–1340.

Straight, S.W., J.N. Pieczynski, E.L. Whiteman, C.J. Liu, and B. Margolis. 2006. Mammalian lin-7 stabilizes polarity protein complexes. *J. Biol. Chem.* 281:37738–37747.

Tabuse, Y., Y. Izumi, F. Piano, K.J. Kemphues, J. Miwa, and S. Ohno. 1998. Atypical protein kinase C cooperates with PAR-3 to establish embryonic polarity in *Caenorhabditis elegans*. *Development.* 125:3607–3614.

Tepass, U., C. Theres, and E. Knust. 1990. crumbs encodes an EGF-like protein expressed on apical membranes of *Drosophila* epithelial cells and required for organization of epithelia. *Cell.* 61:787–799.

Tepass, U., G. Tanentzapf, R. Ward, and R. Fehon. 2001. Epithelial cell polarity and cell junctions in *Drosophila*. *Annu. Rev. Genet.* 35:747–784.

Topinka, J.R., and D.S. Bredt. 1998. N-terminal palmitoylation of PSD-95 regulates association with cell membranes and interaction with K⁺ channel Kv1.4. *Neuron.* 20:125–134.

Torres, V.E., P.C. Harris, and Y. Pirson. 2007. Autosomal dominant polycystic kidney disease. *Lancet.* 369:1287–1301.

Van Itallie, C.M., and J.M. Anderson. 2004. The molecular physiology of tight junction pores. *Physiology (Bethesda).* 19:331–338.

Watts, J.L., B. Etemad-Moghadam, S. Guo, L. Boyd, B.W. Draper, C.C. Mello, J.R. Priess, and K.J. Kemphues. 1996. par-6, a gene involved in the establishment of asymmetry in early *C. elegans* embryos, mediates the asymmetric localization of PAR-3. *Development.* 122:3133–3140.

Woods, D.F., and P.J. Bryant. 1991. The discs-large tumor suppressor gene of *Drosophila* encodes a guanylate kinase homolog localized at septate junctions. *Cell.* 66:451–464.

Yu, J., T.J. Carroll, and A.P. McMahon. 2002. Sonic hedgehog regulates proliferation and differentiation of mesenchymal cells in the mouse metanephric kidney. *Development.* 129:5301–5312.

nature neuroscience



# Astrocytes as determinants of disease progression in inherited amyotrophic lateral sclerosis

Koji Yamanaka[1,2], Seung Joo Chun[1], Severine Boillee[1], Noriko Fujimori-Tonou[2], Hirofumi Yamashita[2], David H Gutmann[3], Ryosuke Takahashi[4], Hidemi Misawa[5] & Don W Cleveland[1]

**Dominant mutations in superoxide dismutase cause amyotrophic lateral sclerosis (ALS), an adult-onset neurodegenerative disease that is characterized by the loss of motor neurons. Using mice carrying a deletable mutant gene, diminished mutant expression in astrocytes did not affect onset, but delayed microglial activation and sharply slowed later disease progression. These findings demonstrate that mutant astrocytes are viable targets for therapies for slowing the progression of non–cell autonomous killing of motor neurons in ALS.**

ALS is an adult-onset neurodegenerative disease, characterized by a progressive and fatal loss of motor neurons. Dominant mutations in the gene for superoxide dismutase (*SOD1*) are the most frequent cause of inherited ALS. Ubiquitous expression of mutant *SOD1* in rodents leads to progressive, selective motor neuron degeneration as a result of acquired toxic properties. The exact mechanism responsible for motor neuron degeneration in ALS, however, is not known[1,2]. Mutant damage in the vulnerable motor neurons is a key determinant of disease onset[3], whereas accumulating evidence supports an active role of non-neuronal cells in motor neuron degeneration[3–7]. Evidence with selective gene excision[3] or bone-marrow grafting[5] has demonstrated that mutant SOD1-derived damage in microglia accelerates later disease progression. Despite the importance of astrocyte function, the role of mutant action in astrocytes in disease has not been tested *in vivo*.

To examine whether mutant SOD1 damage in astrocytes contributes to disease, *loxSOD1$^{G37R}$* mice[3], carrying a mutant *SOD1* gene that can be deleted by the action of the Cre recombinase, were mated with *GFAP-Cre* mice (**Fig. 1** and **Supplementary Fig. 1** online), which express both Cre recombinase and β-galactosidase (*LacZ*) under the control of the human GFAP promoter[8]. Mice from these matings that carry the *GFAP-Cre* transgene are denoted as Cre$^+$, whereas mice without it are referred to as Cre$^-$. To determine the cell-type specificity of Cre expression in the spinal cord, *GFAP-Cre* mice were mated to Rosa26 mice, which ubiquitously express a *LacZ* gene that encodes functional β-galactosidase only after Cre-mediated recombination. Although this *GFAP-Cre* transgene is expressed in a subset of neurons in the cerebellum and hippocampus during embryogenesis[9], measurement of β-galactosidase activity (by deposition of a blue reaction product after addition of the X-gal substrate) demonstrated that Cre expression and Cre-mediated recombination was restricted in the spinal cord to GFAP-reactive astrocytes (**Fig. 1a,b**). The efficiency of mutant gene excision in cultured astrocytes from newborn *loxSOD1$^{G37R}$/GFAP-Cre$^+$* mice was ~76% (**Fig. 1d,e**), determined by quantitative PCR for human SOD1 transgene number (**Fig. 1d**) and immunoblotting for mutant SOD1 levels (**Fig. 1e**). We observed neither detectable Cre activity nor mutant gene excision in microglia (**Fig. 1c** and **Supplementary Fig. 2** online).

A simple, objective measure of disease onset and early disease was applied by initiation of weight loss, itself reflecting denervation-induced muscle atrophy. Reduction of SOD1$^{G37R}$ in astrocytes did not slow disease onset nor early disease (GFAP-Cre$^+$, 341.6 ± 48.9 d; GFAP-Cre$^-$, 337.0 ± 35.8 d; **Fig. 1f,h**). However, late disease progression (from early disease to end stage) was sharply delayed, providing a mean extension of survival by 48 d (Cre$^+$, 87.4 d; Cre$^-$, 39.5 d; **Fig. 1j**). Progression from onset to early disease was more modestly slowed by 14 d (Cre$^+$, 99.3 d; Cre$^-$, 85.2 d; **Fig. 1i**). Overall survival was extended by 60 d (Cre$^+$, 436.5 ± 38.8 d; Cre$^-$, 376.5 ± 26.9 d; **Fig. 1g**). This contrasts with delayed disease onset from diminished mutant synthesis solely within motor neurons (with a *VAChT-Cre* transgene carrying the motor neuron–specific vesicular acetylcholine transporter promoter) without affecting disease progression (**Supplementary Results, Supplementary Methods** and **Supplementary Fig. 3** online), just as reported previously with an *Isl1* (*Islet1*)*-Cre* transgene that is expressed in motor neurons and some peripheral tissues[3].

Astrocytic and microglial cell activation is a well-accepted feature of SOD1 mutant–mediated ALS[1,2]. An elevated proportion of GFAP-positive astrocytes appeared before disease onset (**Fig. 2a**) in *loxSOD1$^{G37R}$* mice. This astrogliosis was progressive, readily apparent by onset (**Fig. 2b**) and more prominent during disease progression (**Fig. 2c**). Despite substantial mutant reduction, astrogliosis was not, however, different in comparing disease-matched *loxSOD1$^{G37R}$/GFAP-Cre$^+$* mice (**Fig. 2d,e**) and *loxSOD1$^{G37R}$/GFAP-Cre$^-$* mice (**Fig. 2b,c**).

Microglial activation occurred at earliest disease onset in *Cre$^-$* mice (**Fig. 2g**) and was progressively more prominent during disease progression (**Fig. 2h**). Microglial activation was, however, substantially delayed from onset through early disease in the *GFAP-Cre$^+$* mice when mutant SOD1 levels were reduced only in astrocytes (**Fig. 2i,j**). By exploiting the presence of β-galactosidase to mark astrocytes with diminished SOD1 mutant synthesis, examination of sections throughout lumbar spinal cords of symptomatic *loxSOD1$^{G37R}$/GFAP-Cre$^+$* mice

[1]Ludwig Institute for Cancer Research and Department of Medicine and Neuroscience, University of California at San Diego, 9500 Gilman Drive, La Jolla, California 92093-0670, USA. [2]Yamanaka Research Unit, RIKEN Brain Science Institute, 2-1 Hirosawa, Wako, Saitama 351-0198, Japan. [3]Department of Neurology, Washington University School of Medicine, 660 South Euclid Avenue, St. Louis, Missouri 63110, USA. [4]Department of Neurology, Graduate School of Medicine, Kyoto University, 54 Shogoin Kawahara-cho, Sakyo-ku, Kyoto 606-8507, Japan. [5]Department of Pharmacology, Kyoritsu University of Pharmacy, 1-5-30 Shibakoen, Minato-ku, Tokyo 105-8512, Japan. Correspondence should be addressed to D.W.C. (dcleveland@ucsd.edu) or K.Y. (kyamanaka@brain.riken.jp).

Received 26 November 2007; accepted 7 January 2008; published online 3 February 2008; doi:10.1038/nn2047

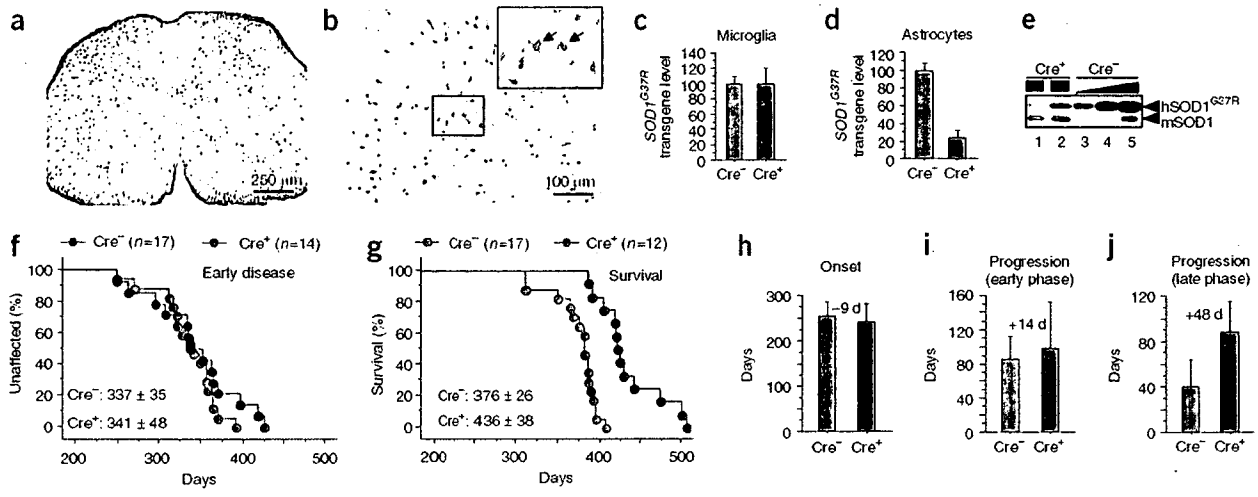


**Figure 1** Selective Cre-mediated gene excision shows that mutant SOD1 action in astrocytes is a primary determinant of late disease progression. (**a**,**b**) β-galactosidase (β-gal) activity in astrocytes in whole (**a**) or in the anterior horn region (**b**) of the lumbar spinal cord section of *GFAP-Cre*/Rosa26 reporter mice visualized with X-gal and immunostaining with GFAP antibody. Inset, magnified image of the boxed area in **b**. Arrows indicate β-gal/GFAP-Cre–expressing astrocytes. (**c**,**d**) *loxSOD1*$^{G37R}$ transgene levels ($n = 3$ for each group) in primary microglia (**c**) or astrocytes (**d**) from *loxSOD1*$^{G37R}$/*GFAP-Cre*$^{+}$ and *loxSOD1*$^{G37R}$ mice using real-time PCR. (**e**) We determined SOD1$^{G37R}$ and mouse SOD1 levels by immunoblotting extracts from isolated primary astrocytes of *loxSOD1*$^{G37R}$/*GFAP-Cre*$^{+}$ (lanes 1, 2) and a dilution series of a comparable extract from LoxSOD1$^{G37R}$ astrocytes representing 25%, 50% and 100% of the protein amounts loaded in lanes 1 and 2 (lanes 3–5). (**f**,**g**) Ages at which early disease phase (to 10% weight loss, $P = 0.76$; **f**) or end-stage disease ($P < 0.0001$; **g**) were reached for *loxSOD1*$^{G37R}$/*GFAP-Cre*$^{+}$ mice (red) and *loxSOD1*$^{G37R}$ littermates (blue). Mean ages ± s.d. are provided. (**h**–**j**) Mean onset ($P = 0.47$) (**h**), mean duration of early disease (from onset to 10% weight loss, $P = 0.35$; **i**) and a late disease (from 10% weight loss to end stage, $P < 0.0001$; **j**) for *loxSOD1*$^{G37R}$/*GFAP-Cre*$^{+}$ (red) and *loxSOD1*$^{G37R}$ littermates (blue). At each time point, *P* value was determined by unpaired *t*-test. Error bars denote s.d.

revealed an inverse relationship (**Fig. 3a–g**) between the number of astrocytes with reduced mutant SOD1 (*Cre*$^{+}$) and activated microglia (correlation coefficient, $r = -0.868$, $P < 0.001$), despite comparable astrocytic activation. Thus, microglial activation was most prominent in areas with the highest mutant SOD1–expressing astrocyte concentration.

Elevated production of nitric oxide by upregulated inducible nitric oxide synthase (iNOS) has been reported in mutant SOD1 mice[10], although deletion of the iNOS gene has modest[11] or no[12] effect on SOD1-mediated disease. It is not known in which glial cells this nitric oxide is produced in *in vivo* models of ALS, although both microglia and astrocytes have an ability to produce it when stimulated *in vitro*[13]. Triple staining of lumbar spinal cord sections with iNOS, Mac2 and GFAP antibodies (**Fig. 3h–r**) revealed that almost all iNOS-positive cells were Mac2-positive microglia (**Fig. 3n–r** and **Supplementary Fig. 4** online), indicating that activated microglia are the primary cell type producing nitric oxide in this SOD1 mouse model. Diminishing mutant synthesis in astrocytes inhibited iNOS induction in disease-matched, symptomatic SOD1 mice (**Fig. 3h,k**), consistent with substantial inhibition of microglial activation (**Fig. 3i,l**).

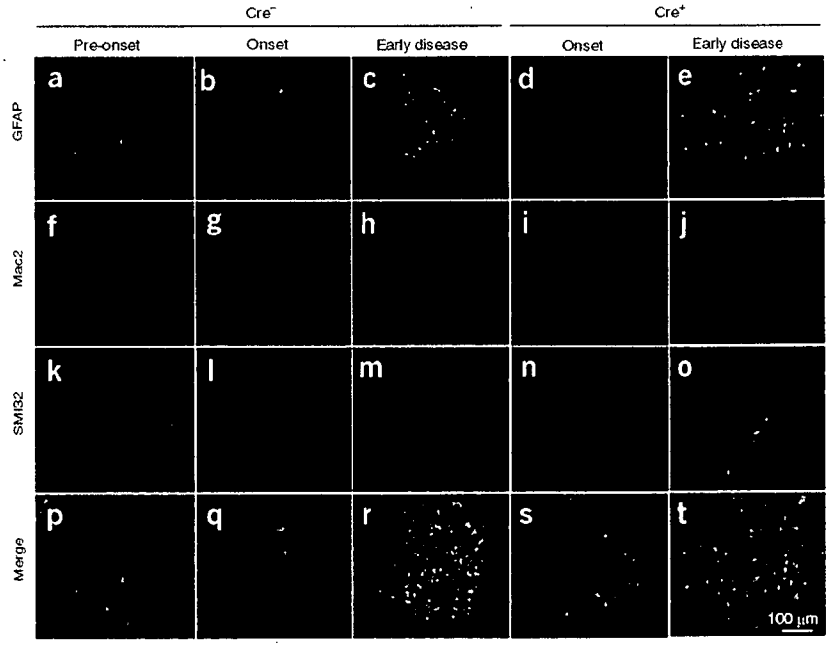


**Figure 2** Selective downregulation of mutant SOD1 in astrocytes significantly inhibits microglial activation. (**a**–**t**) GFAP-positive astrocytes (**a**–**e**), Mac2-positive activated microglia (**f**–**j**) and motor neurons identified with the neurofilament antibody SMI-32 (**k**–**o**) in the lumbar spinal cord of a *loxSOD1*$^{G37R}$ mouse before disease onset (**a**,**f**,**k**,**p**), at disease onset (**b**,**g**,**l**,**q**) or during early disease (**c**,**h**,**m**,**r**), together with *loxSOD1*$^{G37R}$/*GFAP-Cre*$^{+}$ mice at disease onset (**d**,**i**,**n**,**s**) or during early disease (**e**,**j**,**o**,**t**). Merged images are shown in **p**–**t**.

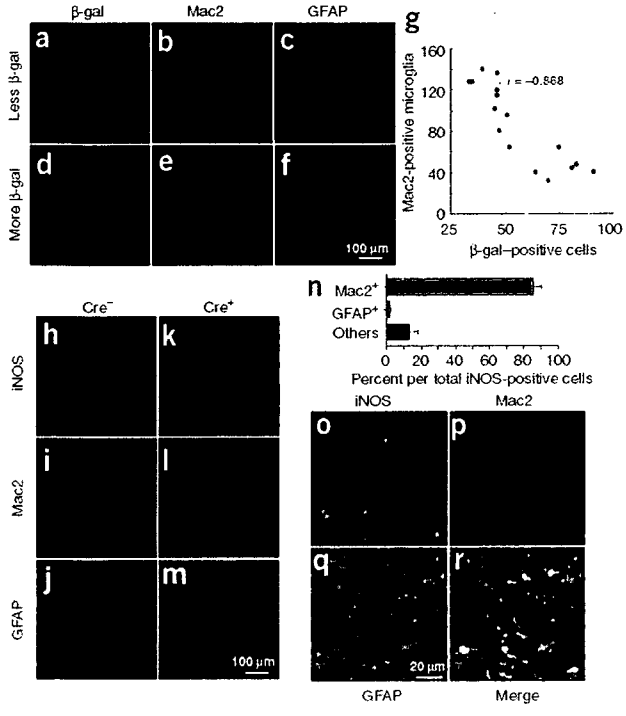


**Figure 3** Mutant-expressing astrocytes enhance microglial activation and induction of iNOS. (**a–f**) Images of β-galactosidase (**a,d**), Mac2 (**b,e**) and GFAP (**c,f**) staining from a left (**a–c**) and right (**d–f**) lumbar spinal cord section from a 12-month-old *loxSOD1*$^{G37R}$*/GFAP-Cre*$^{+}$ mouse. *GFAP-Cre*$^{+}$ astrocytes are marked by β-galactosidase (**a,d**). (**g**) Inverted correlation between the number of Cre-positive astrocytes and Mac2-positive microglia in *loxSOD1*$^{G37R}$*/GFAP-Cre*$^{+}$ mice lumbar spinal cord sections (correlation coefficient, $r = -0.868$, $P < 0.001$). (**h–m**) Lumbar spinal cord sections from *loxSOD1*$^{G37R}$ (**h–j**) and *loxSOD1*$^{G37R}$*/GFAP-Cre*$^{+}$ (**k–m**) mice at the early disease stage immunostained with antibodies to iNOS (**h,k**), Mac2 (**i,l**), and GFAP (**j,m**). (**n**) Quantification of iNOS-positive cells in the anterior horn from lumbar spinal cord of symptomatic *loxSOD1*$^{G37R}$ mice. We plotted the averaged percent of iNOS$^{+}$/Mac2$^{+}$ (red), iNOS$^{+}$/GFAP$^{+}$ (blue) and iNOS$^{+}$/other cell type (black) per total iNOS$^{+}$ cells. (**o–r**) Magnified images of anterior horn from lumbar spinal cord of symptomatic *loxSOD1*$^{G37R}$ mice stained with iNOS (**o**), Mac2 (**p**) and GFAP (**q**). Merged image illustrates that iNOS-positive cells are Mac2-positive microglia (**r**).

A role for astrocytes in inherited ALS has been previously considered in several contexts. Mutant-expressing astrocytes produce and release one or more as yet uncharacterized components that can accelerate motor neuron death *in vitro*[6,7]. Focal loss of the astrocytic EAAT2 glutamate transporter in affected regions[14] (**Supplementary Fig. 5** online) and the failure of normal glutamate uptake of *SOD1*$^{G93A}$ astrocytes *in vitro*[15] support glutamate-dependent excitotoxicity as a component of disease. Nevertheless, diminished mutant SOD1 synthesis in most astrocytes did not affect disease-dependent loss of EAAT2 from those astrocytes (**Supplementary Fig. 5**), indicating that a reduction in glutamate transport reflects non–cell autonomous damage to astrocytes, in part, from mutant SOD1 synthesized by other cells. Our use of selective gene excision has now demonstrated that mutant SOD1 damage in both microglia[3] and astrocytes (**Fig. 1g–j**) accelerates later disease progression without affecting the initiation of motor neuron degeneration and phenotypic disease onset. Discovery that damage in astrocytes determines the timing of microglial activation and infiltration provides further evidence that, beyond any direct effect of mutant astrocytes on motor neurons, such astrocytes amplify an inflammatory response from microglia (including enhanced production of nitric oxide and possibly of toxic cytokines), leading to further damage to the motor neurons and accelerated disease progression through a non–cell autonomous mechanism (**Supplementary Fig. 6** online). These findings validate therapies, including astrocytic stem cell–replacement approaches, that aim to slow disease progression in ALS by supplementing healthy astrocytes or modulating toxicity in astrocytes to control an inflammatory response of microglia.

*Note: Supplementary information is available on the Nature Neuroscience website.*


## ACKNOWLEDGMENTS

This work was supported by a US National Institutes of Health grant (NS 27036) and a grant from the Packard ALS Center at Johns Hopkins (D.W.C.), as well as a Muscular Dystrophy Association developmental grant, the Uehara Memorial Foundation, the Nakabayashi Trust for ALS Research and a grant-in-aid for Scientific Research (19591021) and on Priority Area (19044048) from the Ministry of Education, Culture, Sports, Science and Technology of Japan (K.Y.). Salary support for D.W.C is provided by the Ludwig Institute for Cancer Research. S.B. is a recipient of a Fondation pour la Recherche Medical fellowship, an Institut National de la santé et de la Recherché Medicale fellowship and a Muscular Dystrophy Association developmental grant.


## AUTHOR CONTRIBUTIONS

K.Y., S.J.C., S.B., N.F.-T. and H.Y. conducted the experiments. D.H.G., R.T. and H.M. provided essential experimental tools and advice. K.Y., S.B., and D.W.C. were responsible for the overall design of the project, analyses of the results and writing the manuscript.


Published online at http://www.nature.com/natureneuroscience
Reprints and permissions information is available online at http://npg.nature.com/reprintsandpermissions



1. Pasinelli, P. & Brown, R.H. *Nat. Rev. Neurosci.* **7**, 710–723 (2006).
2. Boillee, S., Vande Velde, C. & Cleveland, D.W. *Neuron* **52**, 39–59 (2006).
3. Boillee, S. *et al. Science* **312**, 1389–1392 (2006).
4. Clement, A.M. *et al. Science* **302**, 113–117 (2003).
5. Beers, D.R. *et al. Proc. Natl. Acad. Sci. USA* **103**, 16021–16026 (2006).
6. Di Giorgio, F.P., Carrasco, M.A., Siao, M.C., Maniatis, T. & Eggan, K. *Nat. Neurosci.* **10**, 608–614 (2007).
7. Nagai, M. *et al. Nat. Neurosci.* **10**, 615–622 (2007).
8. Bajenaru, M.L. *et al. Mol. Cell. Biol.* **22**, 5100–5113 (2002).
9. Fraser, M.M. *et al. Cancer Res.* **64**, 7773–7779 (2004).
10. Almer, G., Vukosavic, S., Romero, N. & Przedborski, S. *J. Neurochem.* **72**, 2415–2425 (1999).
11. Martin, L.J. *et al. J. Comp. Neurol.* **500**, 20–46 (2007).
12. Son, M., Fathallah-Shaykh, H.M. & Elliott, J.L. *Ann. Neurol.* **50**, 273 (2001).
13. Barbeito, L.H. *et al. Brain Res. Brain Res. Rev.* **47**, 263–274 (2004).
14. Howland, D.S. *et al. Proc. Natl. Acad. Sci. USA* **99**, 1604–1609 (2002).
15. Vermeiren, C. *et al. J. Neurochem.* **96**, 719–731 (2006).

Available online at www.sciencedirect.com
ScienceDirect
ELSEVIER
Biochemical and Biophysical Research Communications 356 (2007) 993–997
BBRC
www.elsevier.com/locate/ybbrc

# Evolution of mitochondrial cell death pathway: Proapoptotic role of HtrA2/Omi in *Drosophila*

Tatsushi Igaki [a,1], Yasuyuki Suzuki [b,1], Naoko Tokushige [c], Hiroka Aonuma [d,f], Ryosuke Takahashi [e,*], Masayuki Miura [f,*]

[a] *Department of Genetics, Yale University School of Medicine, Boyer Center for Molecular Medicine, 295 Congress Avenue, New Haven, CT 06536, USA*
[b] *Department of Degenerative Neurological Diseases, National Institute of Neuroscience, National Center of Neurology and Psychiatry, Kodaira, Tokyo 187-8502, Japan*
[c] *Laboratory for Developmental Neurobiology, Brain Science Institute, RIKEN, 2-1 Hirosawa, Wako, Saitama 351-0198, Japan*
[d] *Laboratories for Integrated Biology, Graduate School of Frontier Biosciences, Osaka University, 1-3 Yamadaoka, Suita, Osaka 565-0871, Japan*
[e] *Department of Neurology, Kyoto University Graduate School of Medicine, 54 Shogoin-Kawaharacho, Sakyoku, Kyoto 606-8507, Japan*
[f] *Department of Genetics, Graduate School of Pharmaceutical Sciences, University of Tokyo, 7-3-1 Hongo, Bunkyo-ku, Tokyo 113-0033, Japan*

Received 14 March 2007
Available online 26 March 2007

**Abstract**

Despite the essential role of mitochondria in a variety of mammalian cell death processes, the involvement of mitochondrial pathway in *Drosophila* cell death has remained unclear. To address this, we cloned and characterized DmHtrA2, a *Drosophila* homolog of a mitochondrial serine protease HtrA2/Omi. We show that DmHtrA2 normally resides in mitochondria and is up-regulated by UV-irradiation. Upon receipt of apoptotic stimuli, DmHtrA2 is translocated to extramitochondrial compartment; however, unlike its mammalian counterpart, the extramitochondrial DmHtrA2 does not diffuse throughout the cytosol but stays near the mitochondria. RNAi-mediated knock-down of DmHtrA2 in larvae or adult flies results in a resistance to stress stimuli. DmHtrA2 specifically cleaves *Drosophila* inhibitor-of-apoptosis protein 1 (DIAP1), a cellular caspase inhibitor, and induces cell death both *in vitro* and *in vivo* as potent as other fly cell death proteins. Our observations suggest that DmHtrA2 promotes cell death through a cleavage of DIAP1 in the vicinity of mitochondria, which may represent a prototype of mitochondrial cell death pathway in evolution.


*Keywords:* Apoptosis; Cell death; *Drosophila*; HtrA2/Omi; Mitochondria

Mitochondria play crucial roles in regulating cell death in mammals [1,2]. Upon receipt of apoptotic stimuli, the cell activates caspase protease cascade to execute cell death. The activation of caspases is largely regulated by mitochondrial proteins such as cytochrome *c* (cyt *c*), Smac/DIABLO, and HtrA2/Omi, which are released to cytosol following cell death stimuli [1,2]. cyt *c* directly activates the cytosolic caspase-activating protein Apaf-1, thereby triggering a cascade of caspase activations [1,3]. On the other hand, Smac/DIABLO and HtrA2/Omi indirectly activate caspases by antagonizing inhibitor-of-apoptosis proteins (IAPs), a family of cellular caspase inhibitors [4–7]. HtrA2/Omi, as well as cyt *c*, has also been shown to be important for cell survival, as loss of HtrA2/Omi gene results in a neurodegeneration in mice [8,9].

Despite abundant similarities in cell death mechanisms between vertebrates and flies, the involvement of mitochondria in *Drosophila* cell death machinery has remained unclear. *Drosophila* cell death is largely regulated by three killer proteins Reaper, Hid, and Grim. These proteins are thought to be functional counterparts of mammalian mitochondrial killer proteins Smac/DIABLO and HtrA2/Omi, as they bind to and antagonize IAPs through their

* Corresponding authors.
*E-mail addresses:* ryosuket@kuhp.kyoto-u.ac.jp (R. Takahashi), miura@mol.f.u-tokyo.ac.jp (M. Miura).
[1] These authors contributed equally to this work.

0006-291X/$ - see front matter © 2007 Elsevier Inc. All rights reserved.
doi:10.1016/j.bbrc.2007.03.079